Materials Today Bio 38 (2026) 103094

Contents lists available at ScienceDirect

Materials Today Bio

journal homepage: www.journals.elsevier.com/materials-today-bio

Solid-phase synthesis of high affinity interleukin-6 binders made of gelatin-methacryloyl via a molecular imprinting technique

Devid Maniglio [a,*,1], Alice Marinangeli [b,1], Daniel Moranduzzo [a], Giacomo Canevari [c], Mauro Bonafini [c], Chiara Stranieri [d], Edoardo Di Leo [d], Giorgio Speranza [e], Giandomenico Orlandi [c], Anna Maria Fratta Pasini [d], Alessandra Maria Bossi [b,**]

[a] University of Trento, Department of Industrial Engineering, BIOtech Research Center, Via delle Regole 101, Mattarello, Trento, 38123, Italy
[b] University of Verona, Department of Biotechnology, LaStMolCAL Lab, Strada Le Grazie 15, Verona, 37134, Italy
[c] University of Verona, Department of Computer Science, Strada Le Grazie 15, Verona, 37134, Italy
[d] University of Verona, Department of Medicine, A.O.U.I. Verona, Policlinico GB Rossi, P.le L.A. Scuro 10, Verona, 37134, Italy
[e] Fondazione Bruno Kessler, Center for Sensors and Devices, Via Sommarive, 18, Povo, Trento, 38123, Italy

ARTICLE INFO

Keywords:
Meta-biomaterials
Gelatin methacryloyl
Solid-phase synthesis
Molecularly imprinted polymers
Natural polymers
Interleukin-6
Inflammation

ABSTRACT

Natural polymers can be engineered into nanoscale "molecular traps", the bioMIPs, by the technique of molecular imprinting, which is a template-directed synthesis to generate selective binding sites in a crosslinked matrix. To date, bioMIPs are synthesized in solution by nano-aggregation of the polymeric units around a template, yielding to selective meta-biomaterials. Yet, the in-solution process limits the uniformity and scale-up of the bioMIPs. Here we report the first solid-phase synthesis (SPS) of interleukin-6 (IL-6) selective bioMIPs made of Gelatin methacryloyl (GelMA) and establish design rules for producing monomodal bioMIPs from protein building blocks. SPS synthesis is based on the oriented immobilization of the template to a solid support. SPS nucleation was studied on a plasmonic surface permitting real-time monitoring of bioMIP genesis. Subsequently, it was translated into a prototype reactor for scaling up the production. Guided by Flory-Huggins-De Gennes theory, we mapped the synthetic space by varying GelMA concentration, density and architecture of the surface-immobilized templates, and nucleation-time. The formed SPS bioMIPs were structurally and functionally characterized. Compared with analogous bioMIPs prepared by in-solution imprinting, SPS bioMIPs displayed a low picomolar dissociation constant, surpassing the in-solution ones by 3 orders of magnitude; showed ~1 ng/μg IL-6 uptake in human serum, i.e., ~45-fold increase with respect to in-solution ones, underscoring robust selective recognition under physiologically relevant conditions. Overall, the SPS strategy enables template-free isolation of high-quality bioMIPs and provides a practical route toward manufacturing cytokine-targeting nanotraps for inflammation-modulating biomedical applications.

1. Introduction

Natural polymers can be engineered into nanoscale "molecular traps" through the technique of molecular imprinting (MI) [1–3], which relies on template-directed syntheses to generate selective binding sites within a crosslinked matrix [4–6]. Initially conceived for synthetic polymers [4–6], the MI templating process endows the emerging material with defined molecular recognition properties, effectively converting it into a selective metamaterial. Among the advantages, the MI process has a straightforward synthesis, tunable selectivity, long-term stability and reusability of the formed recognition materials [7].

When the MI technology is applied to naturally derived polymers, it provides a notable route to form unprecedented meta-biomaterials, including customizable "molecular traps" capable of targeting a wide range of molecular species [8]. The resulting bio-based selective binders

Abbreviations: GelMA, Gelatin Methacryloyl; bioMIP, biological molecularly imprinted polymer; SPS, solid-phase synthesis; IL-6, interleukin-6.

* Corresponding author
** Corresponding author
E-mail addresses: devid.maniglio@unitn.it (D. Maniglio), alessandramaria.bossi@univr.it (A.M. Bossi).
[1] Authors shared equal contribution.

https://doi.org/10.1016/j.mtbio.2026.103094
Received 29 January 2026; Received in revised form 25 March 2026; Accepted 2 April 2026
Available online 10 April 2026

are termed "biological molecularly imprinted polymers", or "bioMIPs" [1–3]. Remarkably, this approach couples an exceptionally simple synthetic process with the intrinsic biocompatibility, biodegradability, and non-toxicity of natural polymers, thereby satisfying essential requirements for clinical translation, such as systemic administration, while offering a cost-effective fabrication. The convergence of ease of production and biological safety highlights the distinctive advantages of bioMIPs as biomedical materials and opens an unprecedented landscape of future applications encompassing the scavenging of signal molecules, drug delivery, wound healing, and intelligent scaffolds.

In this context, protein-derived biomaterials fit key requirements of the MI process, making them ideal candidates for the preparation of target-selective meta-biomaterials. Indeed, numerous proteins are available for the process, providing a wide variety in amino acid sequence, which is crucial for the molecular recognition of the intended target molecule. Moreover, proteins display a propensity to entangle into nanogels, especially when unfolded [9], driving the nucleation of the bioMIP and, ultimately, governing its size. Along this line, silk fibroin and gelatin, which are renowned for their biocompatibility, non-toxicity, and approved for use in tissue engineering and regenerative medicine [10,11], were tested as fundamental building blocks in the MI synthesis [1–3]. To prepare the bioMIPs, the chosen natural building block, i.e. polymerizable gelatin (GelMA [12]) or silk fibroin (SilMA [13]), have been employed in diluted conditions (i.e. from 0.03 to 3 mg/mL), with protocols optimized by surface response methods [1,3,14], so as to promote the "nucleation" of individual bioMIPs, maintaining sufficient separation between growing nano-aggregates and thereby preventing their coalescence [15]. As a result, the bioMIP moulds by nano-aggregation of the GelMA-, or SilMA-, units around the defined template.

The formation of bioMIPs in solution proceeds as a statistically governed thermodynamic self-assembly process, whereby natural polymer chains spontaneously organize into entangled nanoaggregates around the template molecule. Templated assemblies occur in dynamic equilibrium with non-templated self-assemblies, leading to the concomitant formation of both bioMIPs and nanoparticles lacking fully defined or high-fidelity recognition sites. The subsequent photopolymerization of the unsaturated pendant double bonds stabilizes these nanoaggregates, yielding crosslinked nanoparticles with hydrodynamic diameters in the range of approximately 50–100 nm [1,3]. Prior to the use, the in-solution synthesized bioMIPs undergo template removal, which is achieved through extensive washing steps, based on dialysis [1,3,15]. Overall, process generates bioMIPs exhibiting high binding affinity (i.e. nanomolar K_D) and a marked target selectivity.

As an example, in-solution synthesized gelatin methacryloyl (GelMA) bioMIPs, designed to recognize the C-terminal epitope of the pro-inflammatory cytokine interleukin 6 (IL-6Cterm), successfully demonstrated to scavenge interleukin-6 (IL-6) in an inflammatory cell model [3]. Interleukins (ILs), particularly IL-6, are key regulators of immune and inflammatory responses, and their dysregulation—especially elevated IL-6 levels—drives acute and chronic inflammatory diseases and poor clinical outcomes [16–19], making selective IL-6 sequestration a promising therapeutic strategy [20,21]. In the chosen inflammatory THP-1 cell model, the IL-6-selective GelMA-based bioMIPs sequestered IL-6 in a dose-response manner, while showing no toxic effect, nor apoptotic or pre-apoptotic effects, even when administered at concentrations up to 2 mg/mL, suggesting possible therapeutic roles for these nanoscaled gelatin-based meta-biomaterials [3].

In the context of therapeutic applications, a critical assessment of the current in-solution bioMIP synthetic process reveals several limitations that warrant optimization. A primary concern is the intrinsic heterogeneity of the resulting nanoparticle population, which arises from the stochastic nature of the thermodynamically driven self-assembly process. Under the in-solution preparation strategy, bioMIP formation is not deterministically controlled, and a fraction of the nanoparticles lack well-defined or functional recognition sites. Yet product homogeneity must be rigorously ensured for clinical translation. The manufacturing process should yield a uniform population of bioMIPs in which each nanoparticle contains defined and functional binding cavities capable of specific target recognition. Achieving such consistency is essential to ensure reproducible bioactivity, predictable pharmacological performance, and regulatory compliance. Additionally, the dialysis-based extraction of the template does not ensure complete removal, potentially leaving residual template molecules entrapped within the polymer network. Instead, residual templates must be absent from the final product for therapeutic applications. Finally, the synthetic process should be scalable, while ensuring batch-to-batch reproducibility.

The requirements of homogeneity, lack of residual template, and scalability can be addressed by radically modifying the synthetic approach, switching from in-solution to a solid-phase synthesis (SPS) method [22–24]. The solid-phase strategy covalently fixes the template to a solid support through coupling chemistries [25,26], ensuring a directional and uniform orientation of the templates exposed on the support, and the covalent anchorage of the template to a solid surface, thereby avoiding template-leakage issues. Next, the monomer solution is added to the support and nanoscale-sized MIPs grow around the grafted templates, triggered by photo- or chemical initiation of the polymerization. At the completion of the process, mild washings are used to remove polymer aggregates and poor binders from the support. Ultimately, nanoMIPs are recovered by an affinity separation step [22,26], or by a thermal gradient [24,27]. Eluted nanoMIPs are a product with more uniform binding characteristics, possessing directional molecular recognition sites. The obtained nanoMIPs are free of template and demonstrate high affinity for the target molecule [24]. SPS marked a revolutionary advancement in MI technology by enabling the production of synthetic polymers with uniform, high-affinity binding sites with enhanced specificity and reproducibility.

Building upon the foundation principles of the SPS methods [24,27], the present study translates for the first time the solid-phase approach to the fabrication of bioMIPs made from natural polymer building blocks. Shifting from solution-phase synthesis to SPS of bioMIP nanoparticles introduces a series of interconnected fundamental and technical challenges rooted in interfacial chemistry, mass transport, and process engineering. In SPS, the template must first be immobilized onto a solid support, controlling its orientation, surface density, structural integrity and accessibility. Polymerization then occurs near a solid–liquid interface, where restricted monomer diffusion and heterogeneous local environments can lead to uneven growth and broad particle size distributions. A key bottleneck is preventing unwanted bulk nucleation in solution, while promoting polymer formation exclusively (or mostly) around the immobilized template, which requires tight control over monomers concentration, and reaction conditions. Altogether, while SPS offers advantages in terms of no template leakage and binding sites homogeneity, substantial challenges related to surface-controlled polymerization, interfacial thermodynamics, reproducibility, should be entirely investigated for the SPS preparation of bioMIPs. In the present work, we investigated the translation of the SPS approach to the preparation of IL-6 selective gelatin-based bioMIPs. Supported by the theory of *Flory-Huggins-De Gennes* [28–30], the synthetic space was explored for parameters including the GelMA concentration, the quantity and quality of nucleation sites at the solid–liquid interface, and the nucleation time, so to optimize the conditions for the formation of uniform monomodal bioMIP nanoparticles. Solid phase synthesized bioMIPs were characterized both physically and functionally, and ultimately employed to scavenge the IL-6 cytokine in human serum.

It is anticipated that the herein proposed bioMIP SPS strategy combines the robustness, scalability and imprinting precision of solid-phase approaches with the biocompatibility of natural polymers. BioMIPs prepared by SPS displayed superior recognition when compared to bioMIPs formed *via* in-solution synthesis. SPS bioMIPs actively bound IL-6 in serum samples, thereby opening new avenues for the production of biologically compatible molecular recognition systems to attenuate

inflammation.

2. Results and discussion

2.1. Conditions for the nucleation of bioMIPs in solid phase

The conditions for the solid phase synthesis of bioMIPs were defined by monitoring the bioMIP's nucleation process in real-time onto a plasmonic support functionalized with the template (Fig. 1a,b,f). The bioMIP's nucleation was described by the physical information provided by the plasmonic measurements (Fig. 1b), which report real-time changes in the refractive index (RI) at the interface between a metal and a dielectric, in the form of optical resonance shifts and with a sensitivity of 10^{-4} ΔRI [31]. For the experiments, a D-shaped plastic optical fiber ($1 \times 9\,mm^2$) surface plasmon resonance (POF-SPR), mounted on a trenched platform with dimensions equal to $5 \times 9\,mm^2$ and metallized with a gold layer of ~60 nm (SI Section 1, SI Fig. 1.1 [32]), was utilized as a monitoring tool. The gold surface was functionalized with the chosen template (SI Section 2 and 3 [33]), that was the C-terminal peptide of IL-6 (IL-6Cterm [3]), which served as the molecular bait in the imprinting process.

BioMIPs were formed starting from GelMA building blocks [3], which are characterized by sol-gel transition at a specific temperature (T_{gGelMA}). GelMA is gelatin modified by reaction with methacrylic anhydride [24], which introduces pendant double bonds in replacement of ε-amino groups of lysines, making it cross-linkable. When cooled at $T < T_{gGelMA}$, GelMA undergoes sol–gel transition, forming entangled networks, characterized by both disordered intra- and inter-chain interactions and by cooperative transition of coils into helix [34]. Hydrogels, are next stabilized by photocrosslinking of the methacrylol pendant double bonds, yielding to materials with adjustable mechanical properties and controllable biodegradability [35,36]. In this work, GelMA having 80% degree of modification was used [3], T_{gGelMA} was in the range 30-35 °C [37] and $M_n = 85.000$ g/mol (synthesis details in SI Section 4).

Fig. 1a–f schematizes the steps of GelMA nucleation on the solid support. The conditions for the SPS of bioMIPs stemmed from in-solution protocols reported earlier [1–3]. An aqueous GelMA solution (V = 100 μL; quantities varying from 300 μg to 100 ng) was deposited onto the plasmonic platform at the T = 50 °C ($T > T_{gGelMA}$) and let cool to room temperature. BioMIP nucleation would occur in correspondence to the IL-6Cterm-baits immobilized at the surface, when the temperature drops below T_{gGelMA}. Cooling the system below T_{gGelMA} turns water into a poor solvent [28,29], leading to part of the GelMA forming entangled nanoaggregates around the baits. Equally, for $T < T_{gGelMA}$ in the bulk liquid volume, i.e. far from the surface, GelMA molecules are expected to aggregate into imprinting-deficient nanoparticles (GelMA NPs).

The GelMA aggregation occurring at the plasmonic surface produces RI shifting over time within the range of sensitivity of the device (Fig. 1b–d). Before nucleation the plasmonic surface was surrounded by a water environment (RI = 1.333). As nucleation proceeded, the deposition of GelMA (RI ≈ 1.382 [38]) around the templates produced local refractive-index changes (ΔRI) at the interface, leading to a corresponding and proportional optical shift (Fig. 1b–d).

The effects of GelMA concentration, the amount of immobilized IL-6Cterm template that served as molecular baits (Fig. 1a–f), the incubation time, and the washing conditions necessary to elute bioMIPs from the support were investigated. In all experiments, dynamic light scattering (DLS) analysis of each step provided information on the quality of the formed GelMA nanoaggregates (Fig. 1c–e,h). In particular, with the aim of producing bioMIPs of nanometric dimensions having hydrodynamic size of ~100 nm and high homogeneity (PDI ≤0.2), the quality of each nucleation condition was assessed by $Z_{average}$ and PDI parameters (Tables 1 and 2).

In a first set of experiments (Fig. 1a), the plasmonic surface was prepared with an Ångstrom-scale length self-assembled monolayer (SAM) made of lipoic acid (LA; length ~3.3 Å), onto which IL-6Cterm template-baits (length ~3.9 nm) were covalently coupled (details in SI Section 2). The resulting LA-IL-6Cterm surface served as a homogeneous layer of flexible baits.

A few considerations concern the nucleation of bioMIPs on the LA-IL-6Cterm surface.

(1) for a densely packed SAM (approximately 0.5 nm [39]), the maximal density of LAs, hence of carboxylic functionalities available for IL-6Cterm coupling on the plasmonic surface ($A_{surface} = 4.5 \times 10^{13}\,nm^2$) was estimated as:

$$\frac{A_{surface}}{A_{LA}} = \frac{4.5 \times 10^{13}\,nm^2}{(\pi \times 0.5^2)\,nm^2} = 5.73 \times 10^{13} \quad \text{(Eq. 1)}$$

(2) grafting by EDC/NHS chemistry at a surface (SI Section 2), in conditions of steric hindrance, is reported to occur with 30-60% efficiencies [40], therefore considering an arbitrary efficiency of 50%, the maximal number of carboxylic functionalities ready for IL-6Cterm immobilization on the whole surface is estimated as 2.86×10^{13};

(3) for bioMIPs growing up to a diameter of Ø~100 nm, the maximal number of bioMIPs accommodated as a monolayer by the surface was:

$$\frac{A_{surface}}{A_{bioMIP}} = \frac{4.5 \times 10^{13}\,nm^2}{(\pi \times 50^2)\,nm^2} = 5.73 \times 10^{9} \quad \text{(Eq. 2)}$$

(4) being the maximal number of baits 2.86×10^{13}, thus far exceeding the maximal number of bioMIPs occupying the LA-IL-6Cterm surface as a monolayer (5.73×10^9), the formation of multiple binding sites on a single bioMIP is expected;

(5) the moles of bioMIPs required to form a monolayer on the surface were:

$$\frac{N_{bioMIPs}}{N_A} = \frac{5.73 \times 10^{9}}{6.022 \times 10^{23}} = 9.4 \times 10^{-15}\,mol \quad \text{(Eq. 3)}$$

(6) considering as about $2\text{-}2.5 \times 10^6$ g/mol the averaged molecular weight for GelMA bioMIPs, as estimated earlier [3], the quantity of GelMA required for the nucleation of the monolayer of bioMIPs on the bait-provided surface resulted:

$$9.4 \times 10^{-15}\,mol \times 2.5 \times 10^{6} \frac{g}{mol} = 23.5 \times 10^{-9}\,g \quad \text{(Eq. 4)}$$

Hence, the nucleation of a monolayer of bioMIPs on the plasmonic surface required about 23.5 ng of GelMA.

Fig. 1a schematizes the bioMIP's nucleation on the LA-IL-6Cterm plasmonic surface. Nucleation over time was monitored by placing heated GelMA solutions (V = 100 μL; T = 50 °C) both in large excess (300 μg or 50 μg) respect to the GelMA quantity required to nucleate a monolayer (23.5 ng), as well as in a quasi-limiting quantity (100 ng). GelMA was let cool to room temperature and let reach sol-gel equilibrium for up to 60 min. The tested GelMA quantities produced a red-shift on the plasmonic surface (Fig. 1b–d, SI Section 5, Fig. 5.1), reporting an RI increment compatible with nucleation. As an example, Fig. 1d shows the effect of GelMA 100 ng, where a $\Delta\lambda = 0.49 \pm 0.08$ nm was observed between 5 and 20 min.

After 60 min of incubation, the solution covering the plasmonic surface was gently withdrawn, placed in a vial, added of the photoinitiator LAP and polymerized [1,3] to inspect nanoaggregation in the bulk solution (GelMA CTRL NPs). Meanwhile, a 100 μL LAP solution was placed on the plasmonic surface and irradiated for 2 min with an LED source at $\lambda = 365$ nm, so as to crosslink the GelMA nanoaggregates present on the surface (Fig. 1a). After crosslinking, the solution was

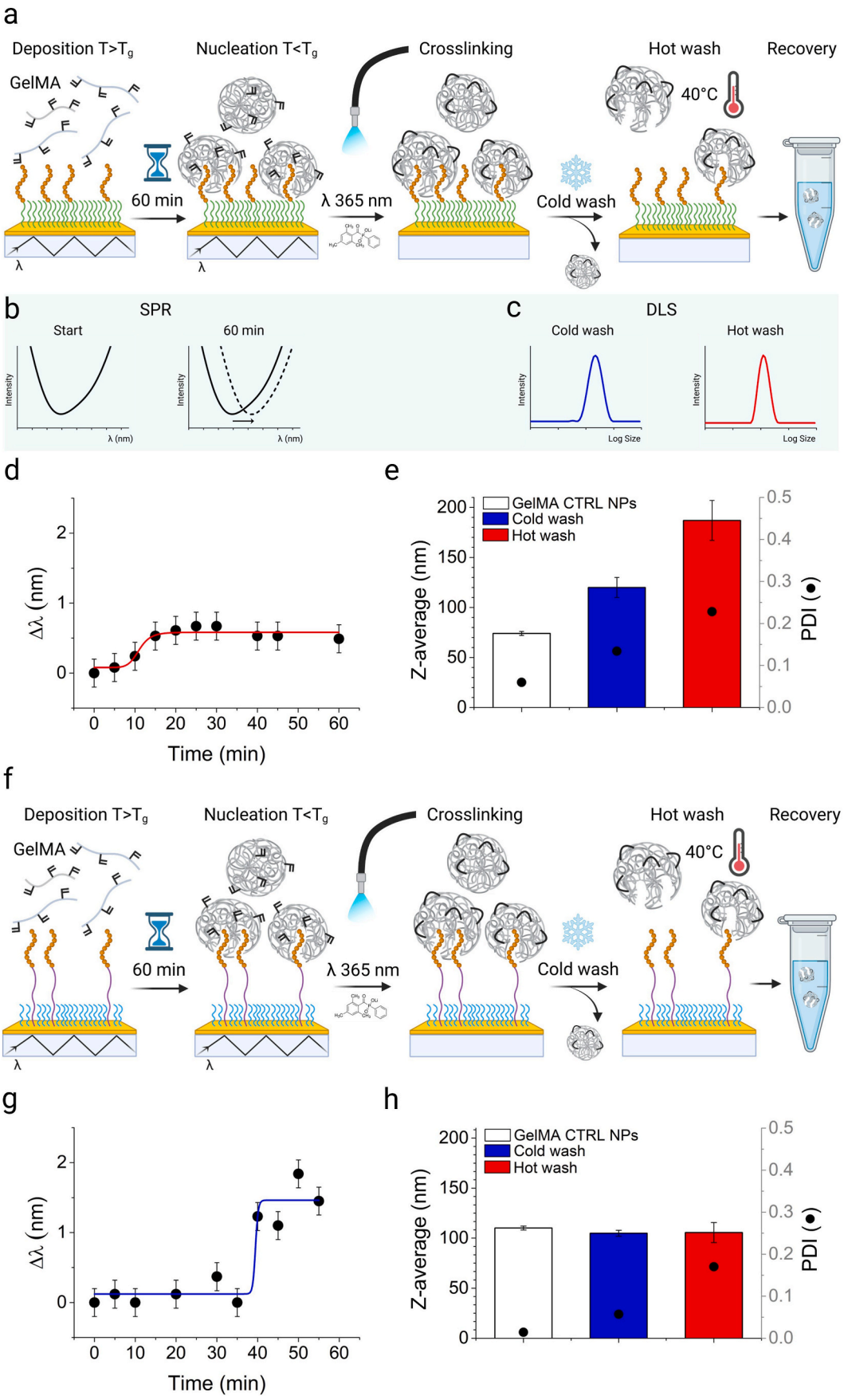

(caption on next page)

Fig. 1. a) schematic of GelMA nucleation steps on a homogeneous LA-IL-6Cterm surface; b) plasmonic signal in the visible wavelength range between 400 nm and 750 nm for GelMA solution 100 ng just deposited on the surface (start) and at the end of the nucleation time (60 min) showing the red-shift of the minimum over the nucleation phenomenon; c) DLS exemplificative profiles of the fractions of GelMA nanoaggregates recovered after cold-wash (blue) and hot-wash (red) (numerical data are reported in Fig. 3 and Tables 1–3); d) plasmonic minimum wavelength variations over time changes for the nucleation of GelMA nanoaggregates on the LA-IL-6Cterm surface, showing a red-shift occurring at 5-20 min, that indicates nucleation; e) bar chart of the Z-average sizes of the GelMA nanoaggregates formed by LA-IL-6Cterm surface nucleation, white bar represents control NPs, blue bar represents cold-wash fraction, red bar represents hot-wash fraction; f) schematic of GelMA nucleation steps on antenna-baits PEG-IL-6Cterm surface; g) plasmonic minimum wavelength variations over time for the nucleation of GelMA nanoaggregates on the PEG-IL-6Cterm surface, showing a steep change is occurring at about 40 min, the reported wavelength change was of about 2 nm, indicating a clear optical effect taking place upon nucleation; h) bar chart of the Z-average sizes of the GelMA nanoaggregates formed by PEG-IL-6Cterm surface nucleation, white bar represents control NPs, blue bar represents cold-wash fraction, red bar represents hot-wash fraction. (For interpretation of the references to colour in this figure legend, the reader is referred to the Web version of this article.)

Table 1
DLS size distributions for GelMA nucleation onto LA-IL-6Cterm surface.

Sample	Z_{ave} (nm)	PDI
GelMA 300 μg		
CTRL NPs	89 ± 3	0.109 ± 0.008
Cold-wash	246 ± 2	0.545 ± 0.016
Hot-wash	560 ± 9	0.434 ± 0.010
GelMA 50 μg		
CTRL NPs	85 ± 2	0.112 ± 0.010
Cold-wash	125 ± 3	0.350 ± 0.030
Hot-wash	332 ± 2	0.321 ± 0.009
GelMA 100 ng		
CTRL NPs	74 ± 2	0.060 ± 0.002
Cold-wash	120 ± 2	0.134 ± 0.004
Hot-wash	187 ± 3	0.228 ± 0.011

Table 2
DLS size distributions for GelMA nucleation onto PEG-IL-6Cterm surface.

Sample	Z_{ave} (nm)	PDI
GelMA 100 ng		
CTRL NPs	110 ± 4	0.017 ± 0.002
Cold-wash	105 ± 3	0.057 ± 0.004
Hot-wash	101 ± 3	0.170 ± 0.009

withdrawn, and the plasmonic surface was washed twice with cold water (cold-wash, 4 °C, < TgGelMA) to remove unbound and weakly adsorbed nanogels. Then, the surface was washed twice with hot water (hot-wash, 40 °C, > TgGelMA), with the aim of detaching and recovering high-affinity GelMA bioMIPs from the baits (Fig. 1a).

Table 3
DLS size distributions for the in-reactor GelMA nucleation.

Sample	Z_{ave} (nm)	PDI
GelMA 12 μg		
CTRL NPs	80 ± 3	0.300 ± 0.020
Cold-wash	519 ± 21	0.510 ± 0.014
Hot-wash	171 ± 3	0.417 ± 0.031

To ensure the effectiveness of the nucleation process and the bioMIP's recovery through an independent experimental approach, nucleation on surfaces was examined using atomic force microscopy (Fig. 2). The pristine IL-6Cterm plasmonic surface presented a streaked topographic profile, suggesting a soft layer of baits (Fig. 2A). By GelMA (100 ng; T = 50 °C) deposition, cooling and crosslinking (Fig. 2B), spherical nanoparticles of sizes of 90-110 nm populated the surface, confirming GelMA nucleation at the surface, in agreement with plasmonics data (Fig. 1d). Following sequential cold and hot wash, the surface appeared devoid of GelMA NPs, suggesting that the vast majority of GelMA nanoaggregates had been harvested and supporting the chosen washing conditions for recovering the bioMIPs (Fig. 2C).

Afterwards, DLS (Fig. 1c) was used to assess the quality of the GelMA nanoaggregates formed in bulk solution (GelMA CTRL NPs), used as a reference, or recovered from the cold and the hot washes (Fig. 1e–. Fig. 3, Table 1). Passing from GelMA 300 μg to 100 ng, the GelMA CTRL NPs hydrodynamic sizes passed from 89 to 74 nm and the PDIs from 0.109 to 0.070 (Fig. 3, column 1; Table 1), resulting in nanogels of striking high homogeneity (PDIs ≤0.1) and dimensions alike previous reports [3]. It can be hypothesized that in solution, GelMA chains entangle driven by the physicochemical characteristics of system (T, T_{gGelMA}, solvent's parameters) [28], with a nanoaggregation process that has similarity to protein's collapse in poor solvating conditions [41,42].

Concerning the cold washes, these were meant to remove loosely interacting GelMA nanoaggregates from the surface. DLS reported size heterogeneity and PDIs inversely correlated with the GelMA concentration, i.e. from Ø = 246 nm and PDI = 0.545 for 300 μg, to Ø = 120 nm and PDI = 0.134 for 100 ng (Fig. 3, column 2, Table 1). The heterogeneity observed for high GelMA quantities possibly suggests that cold washes detach areas of intertwined GelMA nanoaggregates loosely deposited at the surface. When the GelMA concentration approaches its limiting value, each nanoaggregate grows independently, with few to no contact with its neighbors. Finally, hot-washes (T > T_{gGelMA}) were meant to harvest the high affinity bioMIPs from the LA-IL-6Cterm surface

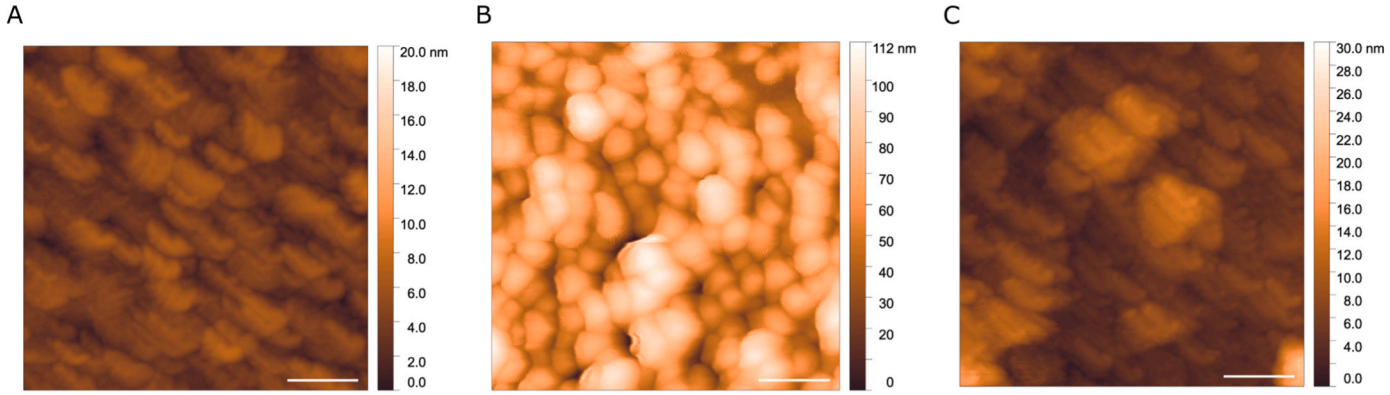

Fig. 2. AFM images of the IL-6Cterm plasmonic surface. (A) The IL-6Cterm functionalized surface, prior to the addition of GelMA, appears streaked, suggesting flexible baits. (B) At the completion of the nucleation and crosslinking of GelMA 1 μg/mL, the surface is covered by GelMA nanoaggregates of size around 90 nm. (C) After hot-washes, the surface appears devoid of GelMA nanoaggregates, suggesting their full removal. White scale bar represents 100 nm.

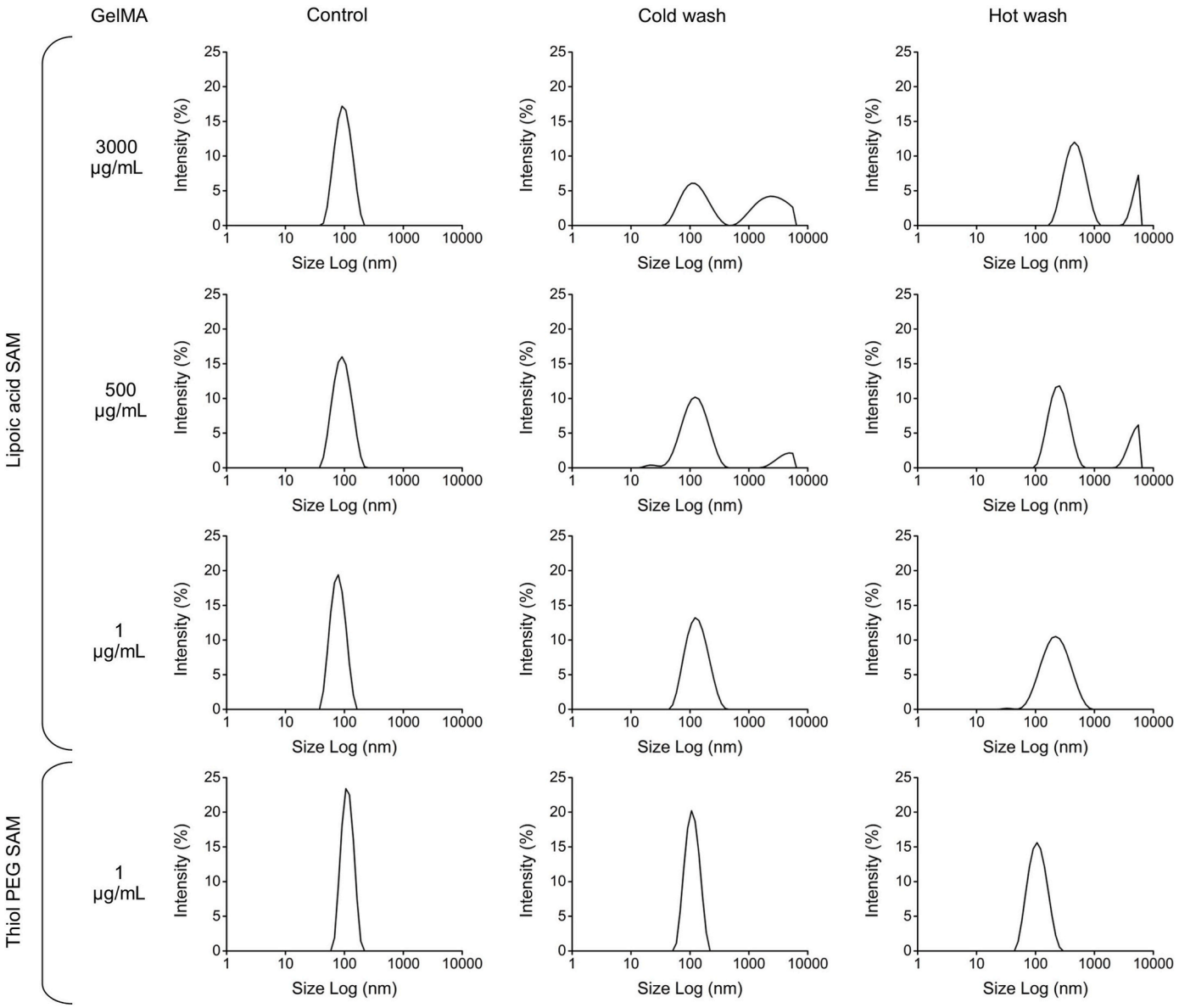

Fig. 3. Dynamic light scattering (DLS) size distribution profiles of GelMA nanoaggregates nucleated on the plasmonic surfaces. Seeding concentrations of 3000, 500, and 1 µg/mL of GelMA, respectively corresponding to 300 µg, 50 µg and 100 ng, were placed on the bait-functionalized surfaces. Rows 1-3 show the size distributions of GelMA CTRL NPs, cold wash, and hot-wash fractions after nucleation and crosslinking onto LA-IL-6Cterm surface. Row 4 shows the size distributions of respectively GelMA CTRL NPs, cold-wash, and hot-wash fractions after nucleation and crosslinking onto PEG-IL-6Cterm surface.

(Fig. 3, column 3). Large and more heterogeneous nanoaggregates (Ø = 560 nm and PDI = 0.434) were reported for GelMA 300 µg, suggesting that seeding an excess of GelMA molecules led to intertwined aggregates nucleated at the surface. Instead, for 100 ng of GelMA, hot water-recovered nanoaggregates had Ø = 187 nm and PDI = 0.228, suggesting that discrete nucleation was favored in GelMA, limiting concentrations.

GelMA nanoaggregates recovered by hot washes were expected to be the solid-phase synthesized bioMIPs, imprinted due to nucleation around the baits. Driving force of the SPS bioMIPs is predicted to be primarily the interactions between GelMA and the template bait [43], then followed by GelMA-GelMA inter- and intra-chain interactions, governed by desolvation and entanglement [44]. For this, the quantity of baits on the nucleation surface and their accessibility might represent a crucial variable.

To investigate the effects of the bait's density and accessibility on the formation of bioMIPs, the plasmonic gold surface was functionalized with a SAM made with a 1:20 mol:mol ratio of thiol-PEG_{12}-COOH, which has an estimated length of ~4.7 nm, respect to thiol-PEG_4-OH, which has length of ~1.8 nm (Fig. 1f). Considering the PEGs to be fully flexible on the surface, using their length as gyration radius (R_g), the total number of PEG_{12}-COOH and PEG_4-OHs was estimated:

$$\frac{A_{surface}}{20 \times A_{PEG4} + A_{PEG12}} = \frac{4.5 \times 10^{13}\ nm^2}{(20 \times (\pi \times 1.29^2))\ nm^2 + (\pi \times 2.21^2)\ nm^2} = \frac{4.5 \times 10^{13}\ nm^2}{(104.56 + 15.34) nm^2} = 3.75 \times 10^{11} \quad \text{(Eq. 6)}$$

PEG_{12}-COOH occupied 12% of the area when compared to PEG_4-OH (*i.e.* 15.34 nm^2 /(104.56 + 15.34) nm^2); hence, the number of PEG_{12}-COOH on the surface was estimated 4.5×10^{10}. Considering the 50% efficiency for the EDC/NHS coupling chemistry to immobilize the IL-6Cterm baits at the surface, the maximal expected grafted bait's number results 2.25×10^{10}, which divided by Avogadro's number (N_A) corresponds to a maximum of 3.73×10^{-14} mol of IL-6Cterm baits (SI

Section 2).

The PEG-IL-6Cterm surface, with respect to the LA-IL-6Cterm surface, presented fewer baits protruding from the ground layer of PEG_4-OH. It was estimated that the IL-6Cterm-PEG_{12} baits extended into the solvent for ~13 nm, serving as an antenna-bait surface. Being the maximum number of bioMIPs accommodated on the PEG-IL-6Cterm surface as a monolayer 5.73×10^9 (Eq. (2)) and the maximal number of antenna-baits 2.25×10^{10}, the formed bioMIPs were expected to bear more than a single imprinted binding site per particle.

As schematized in Fig. 1f, GelMA nucleation was studied on the PEG-IL-6Cterm surface. GelMA used at 100 ng, which was the optimal condition for forming homogeneous nanoaggregates on LA-IL-6Cterm, is shown in Fig. 3, row 3. The experiment followed the same steps reported above for the LA surface. Upon GelMA deposition, a steep red-shift of the plasmonic wavelength was observed between 35 and 40 min ($\Delta\lambda = 1.24 \pm 0.16$ nm, Fig. 1g), suggesting nucleation. After 60 min of incubation, GelMA solution was gently withdrawn (added of LAP and polymerized as a control). A 100 μL aqueous solution of photoinitiator was added to the plasmonic surface and irradiated for 2 min with an LED source at $\lambda = 365$ nm. After crosslinking, the solution was withdrawn and the plasmonic surface was washed twice with cold water (4 °C, $< T_{gGelMA}$), so as to remove unbound and weakly adsorbed GelMA nanogels. Then, the surface was washed twice with hot water (40 °C, $> T_{gGelMA}$), with the aim to detach high affinity GelMA nanoaggregates from the baits.

DLS size distribution profiles, reported in Table 2, Figs. 1h and 3 row 4, showed extremely uniform GelMA CTRL NPs, lacking imprinted cavities, formed in solution as a control ($Z_{ave} = 110$ nm; PDIs = 0.017). Cold washes removed GelMA nanoaggregates with minimal affinity for the baits. Hot-wash was expected to harvest bioMIPs from the baits, showing materials with $Z_{ave} = 101$ nm and PDI = 0.170. Overall, the PEG-IL-6Cterm surface enabled the formation of GelMA nanoaggregates with superior homogeneity compared to LA-IL-6Cterm, suggesting sparser baits with enhanced accessibility play a central role in the quality of the formed nanoaggregates.

An additional comment concerning the surfaces: for GelMA 100 ng, the nucleation on PEG-IL-6Cterm appeared to occur at higher times with respect to LA-IL-6Cterm (Fig. 1d–g). Because of the known role of PEG in disfavoring non-specific interactions, it might be speculated that on the PEG-IL-6Cterm surface, the nucleation points are restricted to the sole IL-6Cterm baits. To form bioMIPs, GelMA must establish attractive interactions with these baits and nucleate, requiring longer times to reach the equilibrium between nanoaggregates and antenna-baits, with respect to the uniformly attractive surface, represented by LA-IL-6Cterm.

The experimental variables relating to GelMA concentration, T_g, type of bait-modified surface, were then used to simulate the bioMIP nucleation by using *Flory-Huggins-de Gennes*'s theoretical framework for polymeric blends (details in SI file THEORY.pdf) [28–30]. The mathematical modelling took into consideration the behavior of GelMA (Fig. 4, colour red) in aqueous solution (Fig. 4, colour blue) at the interface between solvent and the surface (represented by the bottom line in Fig. 4), considering an inspection space of about 500 nm in length and of about 220 nm depth into the solvent, with an average distance of 70.7 nm between adjacent nucleation sites and periodic boundary conditions on the lateral sides, the temperature lowering below T_g and different GelMA concentrations. The dynamic is governed by a *Cahn--Hilliard*-type system of evolution equations for the GelMA volume fraction and chemical potential, incorporating concentration-dependent interfacial parameters, coupled with constant initial conditions and different choices of boundary conditions. Numerical solutions are obtained *via* a linearly stabilized semi-implicit finite element method,

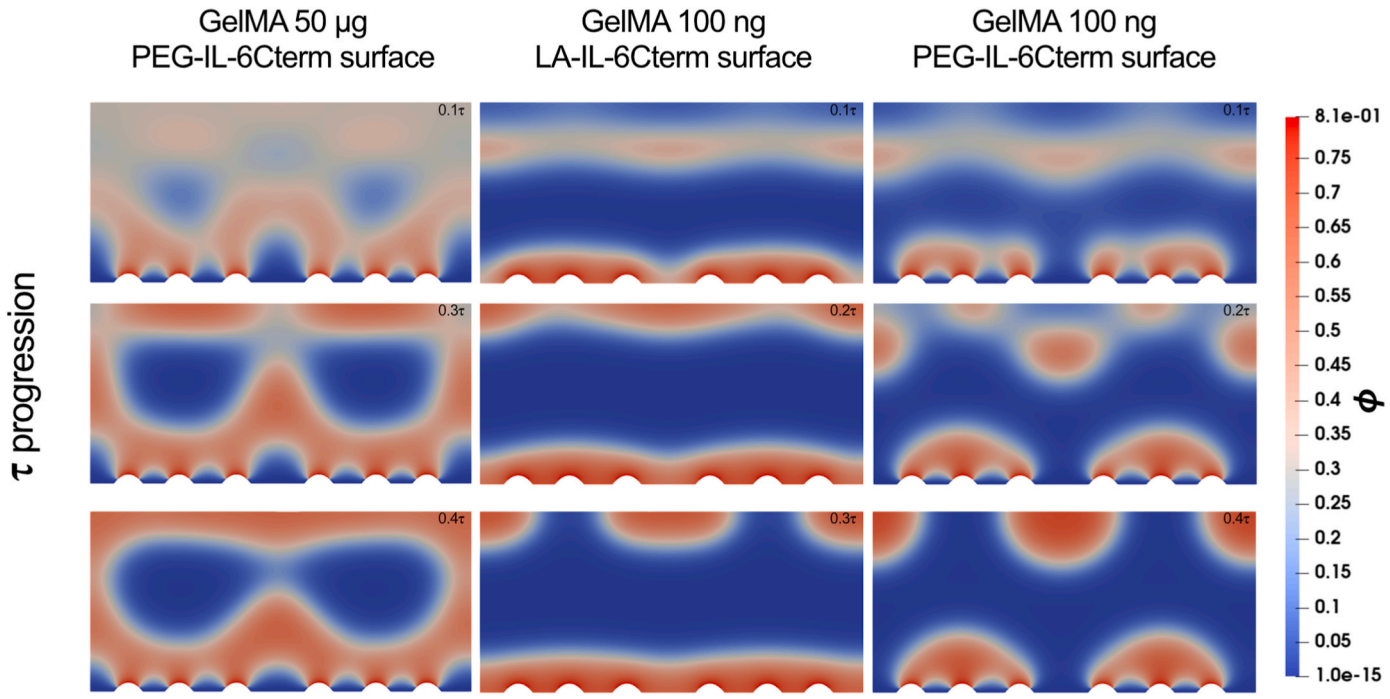

Fig. 4. Mathematical models showing time progression (τ) of the nucleation of excess, 50 μg, GelMA (left column); GelMA 100 ng on LA-IL-6Cterm surface (middle column); GelMA 100 ng on PEG-IL-6Cterm surface (right column). The blue colour represents the solvent; the red colour represents GelMA. Nucleation in the presence of excess GelMA shows the formation of a continuous network of entangled GelMA (red) that aggregates and deposits both on the surface and in the surrounding solution, in agreement with DLS results (Fig. 3, rows 1–2, Table 1). The middle column simulates the nucleation on a homogeneous LA-IL-6Cterm surface with limited GelMA (100 ng), where nanoaggregates initially form as discrete entities and progressively merge into larger structures, in agreement with the PDI value of 0.228 measured by DLS. The right column simulates the nucleation of 100 ng GelMA on the antenna-bait PEG-IL-6Cterm surface, showing enhanced independent nucleation with the formation of individual, multi-bait GelMA bioMIPs at the surface, with sizes ranging from ~170 to 180 nm, consistent with DLS data (Fig. 3, row 4, Table 2). (For interpretation of the references to colour in this figure legend, the reader is referred to the Web version of this article.)

using adaptive time stepping to maintain stability and positivity of the evolving concentration. Full videos of the models are reported as supporting information at the end of the text, while the nucleation process is imaged at defined time frames in Fig. 4. The mathematical modelling describes the temperature-dependent and temporal evolution (τ) of the nucleation process under three distinct conditions: excess GelMA (Fig. 6, left column), 100 ng GelMA on the LA-IL-6Cterm surface (Fig. 6, middle column), and 100 ng GelMA on the PEG-IL-6Cterm surface (Fig. 6, right column). In all simulations, the solvent is represented in blue, whereas GelMA is shown in red. Within the inspected domain (500 nm in length and ~220 nm in depth), the model predicts that an excess of GelMA leads to the formation of a continuous phase, arising from the coalescence of growing nuclei. This behavior results in a non-uniform microstructure, consistent with the high PDI reported in Table 1. For the system comprising 100 ng GelMA on the LA-IL-6Cterm surface, the model simulates high density of nucleation sites distributed across the surface, resembling a carpet-like arrangement. At early times, discrete nuclei are observed (Fig. 4, middle column); however, as τ increases, these nuclei grow and progressively coalesce into larger nanoparticles. The simulated particle size (~200 nm within the 500 nm frame) is in good agreement with DLS measurements (Table 1, 187 ± 3 nm, PDI $= 0.228 \pm 0.011$). In contrast, the model for 100 ng GelMA on the PEG-IL-6Cterm surface (Fig. 4, right column) predicts the formation of isolated, spherical nanoparticles over time. This behavior is consistent with experimental observations, which report a smaller and more uniform population (Table 2, hydrodynamic size $= 101 \pm 3$ nm, PDI $= 0.170 \pm 0.009$). It should be noted that the current simulations are constrained by computational limitations on the size of the inspected domain, which preclude straightforward extraction of statistical descriptors, such as the PDI, for the simulated bioMIP population. Consequently, a direct quantitative comparison with DLS-derived distributions is only attempted. Similarly, direct comparison of nucleation kinetics is not currently possible, as the temporal evolution is expressed in terms of an intrinsic system timescale that depends on a diffusion parameter that has yet to be determined. Nevertheless, the predicted particle size and qualitative morphological features show strong agreement with the experimental results. Overall, mathematical modelling together with the nucleation tests performed on the plasmonic surface provided the set of conditions to scale up the bioMIPs synthesis in the reactor.

2.2. Solid phase synthesis of bioMIPs

The conditions for the SPS of bioMIP's were translated from the real-

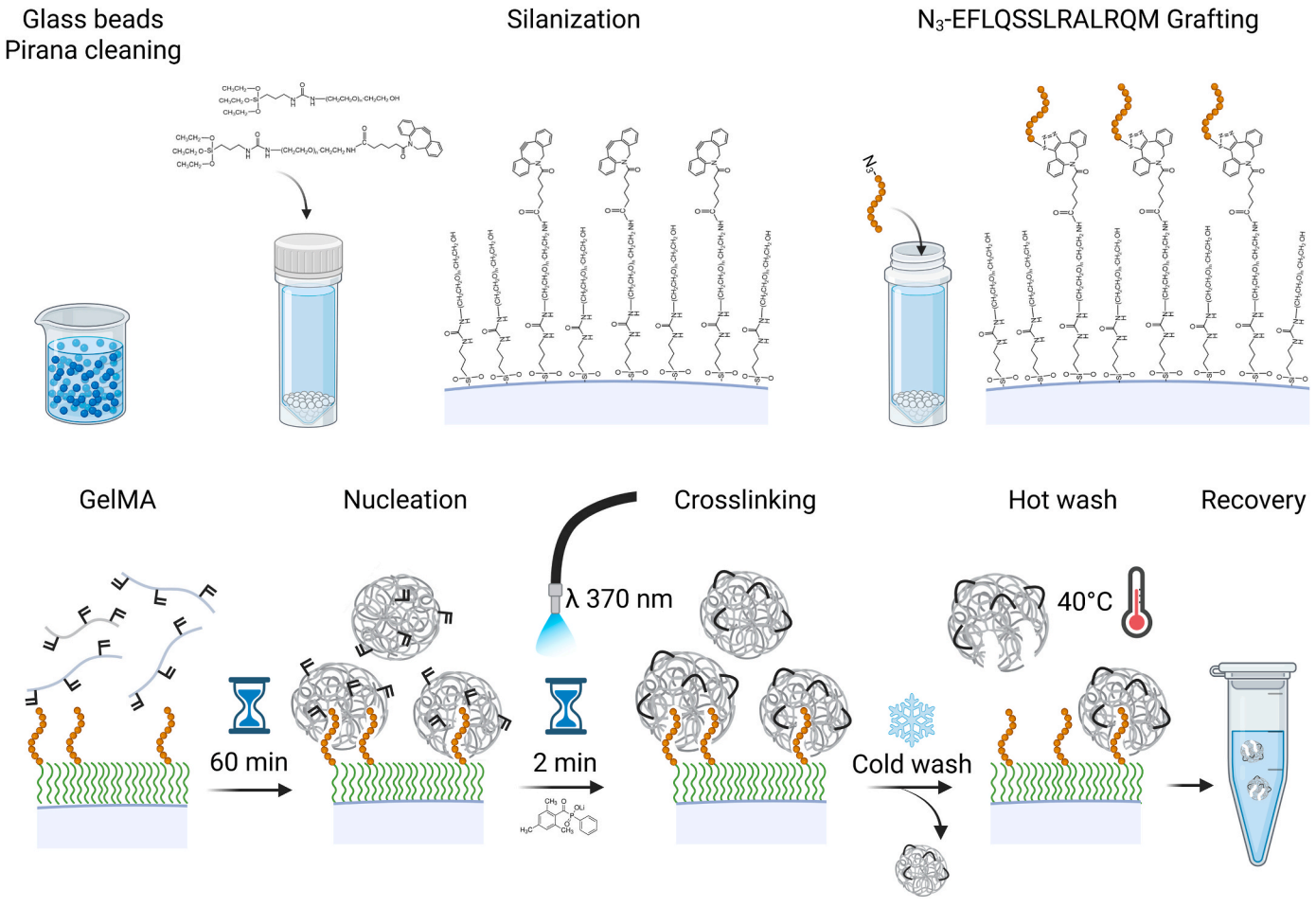

Fig. 5. Schematic of the bioMIP synthesis in the SPS reactor (A-upper panel). For the functionalization of GBs with the IL-6Cterm template, GBs were cleaned with a Piranha solution and treated with NaOH to expose hydroxyl groups. Next, a 1:10 mol:mol ratio DBCO-PEG-silane:PEG-silane was used to silanize GBs and click chemistry was performed to graft an azide derivatized IL-6Cterm template peptide to the DBCO-derivatized GBs. A fixed quantity of IL-6Cterm-GBs was deposited in each reactor plate (N = 6) so as to coat the plate surface with a quasi-monolayer. (B-lower panel) BioMIPs nucleation was performed in the reactor plates (N = 6), by adding 2 μg per reactor-plate of GelMA heated solution (50 °C, > T_{gGelMA}), incubating for 60 min at room temperature, to allow GelMA's nanoaggregation. GelMA solution was recovered, the reactor plates were filled with the photoinitiator solution, and photopolymerization was triggered by a UV LED source. The reactor was then emptied, washed with cold water to recover GelMA nanoaggregates loosely attached to GBs, which supposedly lacked high-affinity imprints. Finally, hot washes were used to recover high-affinity bioMIPs from the reactor.

time plasmonic surface to the model reactor, with the aim of scaling up the synthesis under controlled reaction parameters, ensuring quantitative production of bioMIPs. As a proof of concept, a six-chamber reactor was placed under a UV light source positioned at 10 cm distance. Each chamber had a diameter of ø = 35 mm and was filled with a 2 mL solution volume (SI Section 6).

The SPS protocol was modified from Refs. [25,45]. The steps are schematized in Fig. 5 (upper panel). Glass beads (GBs) were washed in Piranha solution, activated by boiling in NaOH so as to expose the silanols and functionalized with dibenzocycloctyne-PEG-Silane (DBCO-PEG-silane) to introduce terminal reactive DBCO suitable to immobilize an azide-modified IL-6Cterm peptide-template by click chemistry [46]. In particular, the DBCO click chemistry was chosen because it is a copper-free reaction used for bio-orthogonal conjugation. GBs were modified with a mix of DBCO-PEG-silane and PEG-silane used at a ratio 1:20 mol:mol so as to reproduce the condition of "antenna baits". DBCO-PEG reacts with the N_3-labeled peptide-template to form a stable triazole ring, through a strain-promoted azide-alkyne cycloaddition (SPAAC), which does not require a toxic copper catalyst, making it suitable for labeling biomolecules, including in living systems [46,47]. As a result, the N_3-IL-6Cterm template was immobilized onto the GBs with a defined orientation. Additionally, by azide conjugation, the lateral functional groups of the IL-6Cterm peptide, such as ε-NH_2 of lysines, were not involved in the conjugation, allowing them to be free to be involved in the imprinting process so as to attain high fidelity of recognition. To verify that GBs were modified with DBCO-PEG and further with N_3-IL-6Cterm, FT-IR and XPS were performed (SI Section 7).

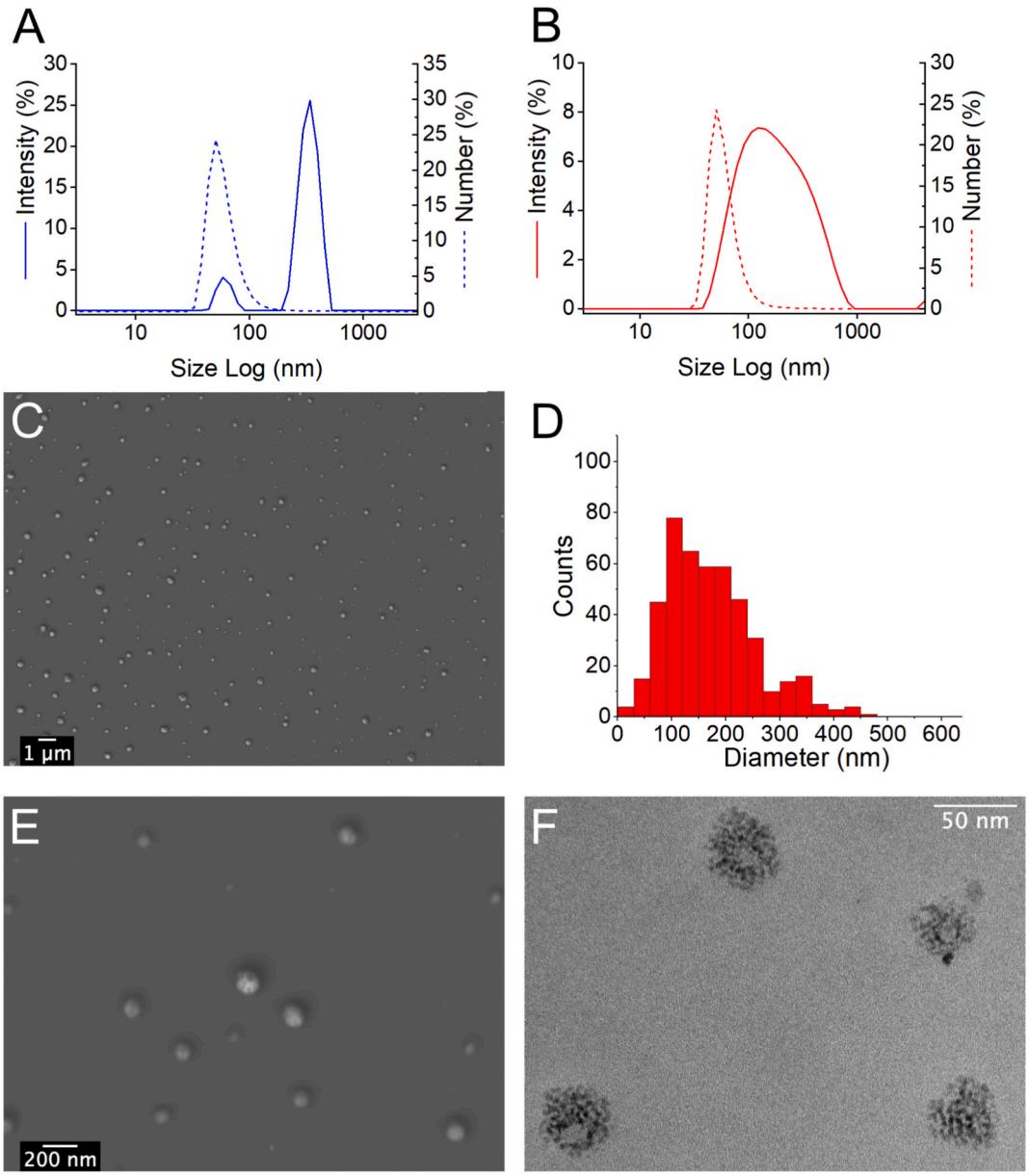

Fig. 6. DLS of the bioMIPs produced in the SPS reactor: (A) cold-wash by intensity (blue line) and by number (blue dotted line); (B) hot-wash by intensity (red line) and by number (red dotted line); (C) SEM image of the hot-wash bioMIPs and (D) size distribution profile of the hot-wash bioMIPs from SEM images (estimated from 342 NPs); (E) SEM image of the hot-wash bioMIPs, larger magnification, showing spherical nanoparticles; (F) insights by TEM image of the density of hot-wash bioMIPs, showing a non-continuous density, suggesting highly structured regions intertwined with low structured regions, so for confirming the nanogel nature of GelMA bioMIPs in coherence with gelatin-based nanomaterials. (For interpretation of the references to colour in this figure legend, the reader is referred to the Web version of this article.)

Next, the quantity of IL-6Cterm-GBs to be packed in a reactor plate was estimated by considering 60 μm as the mean diameter of a GB and 35 mm as the reactor plate diameter. The maximal number of GB accommodated into the reactor plate in a monolayer resulted:

$$\frac{A_{reactor}}{A_{GB}} = \frac{9.62 \times 10^{8}\ \mu m^2}{2.87 \times 10^{3}\ \mu m^2} = 3.35 \times 10^{5} \quad \text{(Eq. 7)}$$

this was further corrected for the geometrical packing factor $\eta = 0.9069$, resulting in 3.04×10^5.

Knowing that an averaged bioMIP of Ø~100 nm has $A_{bioMIP} = (4\pi r^2) = 3.14 \times 10^4\ nm^2$ and that a GB has $A_{GB} = (4\pi r^2) = 1.15 \times 10^{10}\ nm^2$, it follows that the maximal number of bioMIPs on a GB was:

$$\frac{A_{GB}}{A_{bioMIP}} = \frac{1.15 \times 10^{10}\ nm^2}{4.14 \times 10^{4}\ nm^2} = 2.75 \times 10^{5} \quad \text{(Eq. 8)}$$

Supposing that tightly packed GBs would offer less surface available for nucleation, a 2/3 correction factor was introduced to determine the maximal number of bioMIP that nucleates on a single GB:

$$\frac{2/3\ A_{GB}}{A_{bioMIP}} = \frac{2/3\ (1.15 \times 10^{10}\ nm^2)}{4.14 \times 10^{4}\ nm^2} = 1.83 \times 10^{5} \quad \text{(Eq. 9)}$$

The maximal number of bioMIPs produced in each reactor plate was:

$$1.83 \times 10^{5} \frac{bioMIPs}{GBs} \times 3.04 \times 10^{5} \frac{GBs}{plate} = 5.56 \times 10^{10} \frac{bioMIPs}{plate} \quad \text{(Eq. 10)}$$

Each reactor plate was estimated to produce 5.56×10^{10} bioMIPs, which corresponded to 9.24×10^{-14} mol of bioMIPs. Considering 2.5×10^6 g/mol the molecular weight of bioMIPs [3] and 85×10^3 g/mol that of GelMA, the moles of GelMA to form a bioMIP were ~24. Therefore, it resulted that the GelMA required to form a layer of bioMIPs on the IL-6Cterm-GBs in the reactor plate was:

$$9.24 \times 10^{-14}\ mol \times \left(24 \times 85 \times 10^{3} \frac{g}{mol}\right) = 1.88 \times 10^{-7} g \quad \text{(Eq. 11)}$$

Each reactor plate required 188 ng of GelMA to reach a 100% theoretical nucleation. In the present work, the reactor was set up with 6 plates and fed with a total of 12 μg of GelMA, which corresponded to an excess of GelMA of about 9 times, with respect to the quantity required for 100% nucleation.

The in-reactor nucleation process (Fig. 5, lower panel) was performed according to the steps described earlier for the real-time measurements. Briefly, a total quantity of 12 μg of heated GelMA (50 °C, > T_{gGelMA}) was distributed in a 6-plate reactor packed with IL-6-PEG-GBs and incubated at room temperature for 60 min. Next, the GelMA solution was withdrawn, and LAP was added off-reactor for the polymerization, as a control. The reactor plates were filled with an aqueous solution of photoinitiator and irradiated for 2 min with an LED source at $\lambda = 365$ nm. After crosslinking, the solution was removed, and the reactor plates were washed twice with cold water (4 °C, < T_{gGelMA}), so as to remove unbound and weakly adsorbed GelMA nanogels. Then, the reactor plates were washed with hot water (65 °C, > T_{gGelMA}, 10 min under mild shaking) to harvest high affinity GelMA nanoaggregates from the baits.

Samples recovered from in-reactor SPS nucleation were analyzed by DLS (Table 3). GelMA CTRL nanoparticles (NPs) exhibited a relatively uniform population with an average size of approximately 80 nm. Cold washes (Fig. 6A, blue solid line), designed to remove GelMA nanoaggregates with low affinity for the baits, yielded a heterogeneous population characterized by a broad size distribution and a polydispersity index (PDI) of 0.51. In contrast, hot washes (Fig. 6B, red solid line), aimed at recovering high-affinity bioMIPs from the baits, yielded nanoaggregates with an average diameter (Z_{ave}) of 171 nm and a PDI of 0.417. These particles were therefore approximately twice the size of the bioMIPs nucleated on the flat plasmonic surface and displayed lower size uniformity.

Notably, when the number-based size distributions were considered for both cold (Fig. 6A, blue dotted line) and hot washes (Fig. 6D, red dotted line), the dominant nanoparticle population was centered around ~80 nm. This observation suggests that the in-reactor SPS synthesis produces nanoaggregates comparable in size to those obtained on the model plasmonic surface. The broader intensity distributions and higher heterogeneity likely reflect the increased complexity associated with filling, washing, and emptying a confined reactor environment compared with a planar surface system.

The morphology of hot-wash bioMIPs was further examined by scanning electron microscopy (SEM) (Fig. 6C and close-up in Fig. 6E), which revealed predominantly spherical nanoparticles. SEM images were subsequently subjected to statistical analysis to provide independent confirmation of the particle size distribution. As shown in Fig. 6D, the distribution derived from 459 particle counts yielded an average diameter of 170 ± 62 nm, with the most abundant populations falling within the 80–200 nm range. These results are in good agreement with the DLS measurements. Finally, transmission electron microscopy (TEM) was used to assess the internal density of the hot-wash bioMIP nanoparticles (Fig. 6F). The images revealed non-uniform electron density, suggesting highly structured regions intertwined with low structured regions, and consistent with the nanogel nature of the GelMA nanoparticles. At last, to further characterize the reactor's synthetic product, the molecular weight of SPS bioMIPs (hot-wash) was estimated by gel permeation chromatography. SPS bioMIPs have a molecular weight of about 2×10^6 g/mol (details in SI Section 9), which was in fair accordance with in-solution bioMIPs reported elsewhere [3].

2.3. Yield of the in reactor SPS of bioMIPs

The yield of the SPS production of bioMIPs was estimated by analysing the total carbon content (TOC) of each step of the in-reactor synthesis (SI Section 8) when the six-plates reactor was fed with a total of 12 μg of GelMA. Specifically, in the hot-wash a quantity corresponding to 210 ± 33 ng of GelMA nanoaggregates was estimated. From previous calculations, the maximal quantity of GelMA required to saturate the reactor was 188 ng per reactor plate (Eq. (11)), therefore, the yield of the in-reactor SPS synthesis was estimated as follows:

$$Yield\ SPS\ of\ bioMIPs = \frac{Q_{GelMA\ in\ hot-wash}}{N\ plates \times Q_{GelMA\ to\ saturate\ GBs}} \times 100 = \frac{210\ ng}{6 \times 188\ ng} \times 100 = 18.6\ \% \quad \text{(Eq. 12)}$$

The yield of the SPS of bioMIPs, estimated at approximately 19%, is slightly higher respect to the yields reported for nanoMIPs made of polyacrylamides prepared in SPS [24,27].

2.4. Molecular recognition properties of SP nucleated bioMIPs

To verify whether the SPS nucleation forms imprinted bioMIPs capable of selectively recognizing IL-6, the binding abilities of the GelMA nanoaggregates, recovered during the various SPS steps were tested. A fluorescent binding assay was performed, in similarity to what reported in Ref. [3], using a fluorescently labeled IL-6Cterm, i.e. the TAMRA-IL-6Cterm. When the TAMRA-IL-6Cterm binds to a bioMIP, its fluorescence quenches, whereas nonspecific interactions do not alter fluorescence. Therefore, TAMRA-IL-6Cterm (2.5 pmol/well) was incubated with known quantities of GelMA CTRL NPs, or cold-washes, or hot-washes, and compared with known quantities of bioMIPs prepared by the in-solution protocol [3]. Fig. 7A shows that the TAMRA-labeled template was quenched when incubated with bioMIPs prepared by the in-solution synthesis (white bars: 50 ng; striped bar: 500 ng). Quenching did positively correlate with bioMIPs quantity, as expected [3]. When TAMRA-IL-6Cterm was placed in incubation with cold-wash samples (26 ng, blue bar) there was no apparent interaction ($I/I_o \sim 1$), suggesting

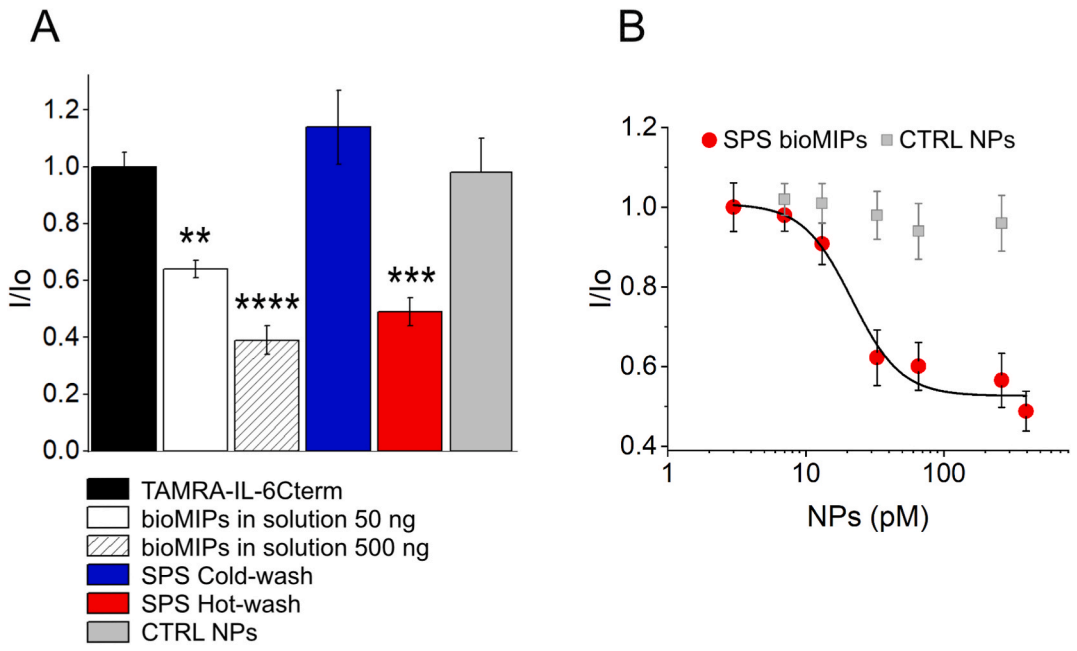

Fig. 7. (A) Fluorescent assay to test the binding properties of bioMIPs prepared by SPS. The labeled template, TAMRA-IL-6Cterm (2.5 pmol, black bar) fluorescence in solution was normalized to 1. The incubation of the TAMRA-IL-6Cterm with in-solution synthesized GelMA bioMIPs as per [3] (white bar 50 ng; striped-white bar 500 ng) resulted in quenching of the fluorescence, indicative of binding. Cold-wash recovered GelMA nanoaggregates (26 ng, blue bar) incubated with the TAMRA-IL-6Cterm did not perturb fluorescence, indicating no binding. In contrast, hot-wash recovered GelMA nanoaggregates (13 ng, red bar) demonstrated significative quenching of the fluorescence of the TAMRA-IL-6Cterm, supporting binding and confirming the imprinting effect on SPS. Control GelMA nanoaggregates, formed in the reactor but not at the surface (grey bar) did also show no binding. Statistical comparisons were performed against CTRL NPs using Dunnett's multiple comparisons test following one-way ANOVA: *p < 0.05; **p < 0.01; ***p < 0.001; ****p < 0.0001. (B) Binding isotherm for SPS bioMIPs (hot-wash fraction, red circle) showed a marked sigmoidal profile and the typical saturation course. Non-linear fitting with Hill model equation permitted to estimate a low picomolar affinity of SPS bioMIPs for the IL-6Cterm template ($R^2 = 0.98322$; $\chi^2 = 0.56997$; fitting parameters in SI Section 10). CTRL NPs (grey square) did not show binding. (For interpretation of the references to colour in this figure legend, the reader is referred to the Web version of this article.)

cold-wash indeed contains GelMA nanoaggregates without imprinting. In contrast, when TAMRA-IL-6Cterm was incubated with hot-washes (13 ng, red bar), a significant decrease in I/I_o was observed, suggesting a strong interaction between the labeled peptide and the hot-wash recovered GelMA nanoaggregates. This evidence permitted us to affirm that bioMIPs with affinity for their template were produced in the reactor solid phase synthesis. As a final control, GelMA nanoaggregates, recovered from the reactor at the end of the 60-min incubation and polymerized outside the reactor were also tested (grey bar), showed an $I/I_o \sim 1$, confirming that nanoaggregates in solution are devoid of IL-6 selective binding.

To estimate the affinity of solid phase synthesized bioMIPs, hot-wash fractions were concentrated and used to study their binding affinity for TAMRA-IL-6Cterm. BioMIPs from hot-wash fraction showed a binding isotherm with a typical saturation course, supporting the presence of a defined number of binding sites and accounting for an effective imprinting in SPS (Fig. 7B). By fitting the experimental data with a Hill model equation, a picomolar apparent dissociation constant (K_{Dapp} 21.65 ± 4.22 pM) was reported, with cooperativity $n = 2.43 \pm 0.84$ (fitting report in SI Section 10). The dissociation constant in the picomolar range indicates an exceptionally strong affinity of the SPS-derived bioMIPs for the template. Notably, this affinity is approximately three orders of magnitude higher (735-fold) than that reported for bioMIPs prepared via conventional in-solution synthesis, for which a dissociation constant of 16.31 ± 1.84 nM was previously measured [3]. Such a marked improvement highlights the intrinsic advantage of the solid-phase synthesis (SPS) approach in controlling the formation of high-fidelity binding sites. This enhancement in affinity is most plausibly attributed to the mechanistic characteristics of SPS. In this process, nucleation occurs directly around immobilized template baits, ensuring that each growing nanoparticle forms in the immediate vicinity of at least one template molecule. As a result, every SPS-derived bioMIP necessarily incorporates at least one imprinted binding site with structural complementarity to the target. In contrast, in-solution polymerization proceeds through stochastic nucleation events that are largely independent of template proximity. This mechanism generates a heterogeneous population comprising both imprinted and non-imprinted GelMA nanoaggregates. Consequently, the experimentally measured affinity represents an ensemble average over particles with widely varying binding capabilities, leading to a substantially lower apparent affinity. The superiority of the SPS approach has been previously documented for other molecularly imprinted nanomaterials. For example, SPS-prepared polyacrylamide MIP nanoparticles targeting trypsin exhibited a threefold reduction in the dissociation constant compared with analogous particles produced via in-solution synthesis [48]. Even more pronounced effects have been reported for small-molecule targets: SPS polyacrylamide MIP nanoparticles designed for D-glucuronic acid displayed a dissociation constant of 800 nM, representing a 245-fold affinity enhancement relative to their in-solution counterparts ($K_D = 196$ μM) [25]. Together with the present results, these observations reinforce the notion that SPS provides a powerful strategy to maximize imprinting efficiency and binding-site fidelity, ultimately enabling the production of synthetic receptors with markedly improved binding performance.

Concerning the Hill parameter n in the fitting equation, this indicates the degree of cooperativity of the binding sites on the same bioMIP. In particular, in Fig. 7B the estimated degree of positive cooperativity was $n = 2.43 \pm 0.84$, which indicates the binding of a first IL-6Cterm molecule to a first bioMIP imprinted site produces a positive effect on the binding of the next IL-6Cterm on another binding site of a same bioMIP. The cooperativity resulting from the fitting is also supported by the multiple binding sites per bioMIP expected by the spatial distribution of

the antennas-bait on the solid support. It is hypothesized that the structural organization of the GelMA bioMIP nanogel network provides the basis for its cooperative behavior. It is anticipated that the imprinted binding sites are located within domains of elevated polymeric entanglement and crosslink density, which maintain the 3D stereochemical fidelity required for IL-6 recognition. Conversely, the intervening, less structured polymer regions connecting these domains may be responsible for cooperative behavior. TEM images (Fig. 6F) showing non-uniform density of the bioMIPs, characterized by lowly structured areas intertwined by highly structured areas, support flexibility and cooperative effects.

The binding of SPS bioMIPs to the full-lenght IL-6 protein was investigated using a competitive fluorescence assay with a rationally selected panel of proteins representative of distinct biological classes. Specifically, competitors were chosen to include both pro-inflammatory cytokines (IL-1β, IL-8, IL-11), so to probe selectivity against structurally or functionally related mediators of inflammation, and pro-regenerative interleukins (IL-4, IL-13), so to assess potential cross-reactivity with cytokines involved in tissue repair. Finally, highly abundant serum proteins, such as human serum albumin (HSA) and human transferrin (HTR), were tested too, so as to evaluate the robustness of the bioMIP system under physiologically relevant conditions. As shown in Fig. 8, IL-6 (purple bar) effectively displaced TAMRA-IL-6Cterm, confirming that the imprinted cavities generated by SPS bioMIPs recognize the full-length cytokine. In contrast, none of the other tested proteins induced very significant displacement, supporting a high degree of selectivity of the SPS prepared bioMIPs. Notably, even IL-11, which shares structural homology with IL-6, did not compete effectively; this behavior may be attributed to differences in physicochemical properties, such as the isoelectric point and hence surface charge distribution of IL-11 (pI = 9.8) with respect to IL-6 (pI = 6.4), which likely affect the interaction with the imprinted binding sites. Collectively, competition results confirm that IL-6Cterm-imprinted SPS bioMIPs exhibit selective recognition of IL-6 even in the presence of structurally related cytokines and abundant serum proteins, supporting their use in physiologically relevant conditions.

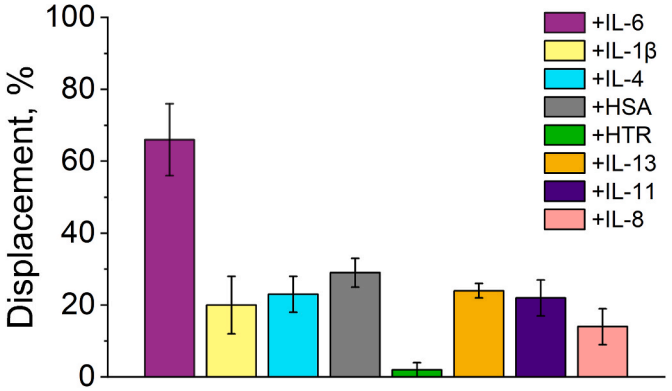

Fig. 8. Selectivity of IL-6 bioMIPs. Selectivity was assessed using a fluorescence competition assay. The fluorescence of TAMRA-IL-6Cterm (2.5 pmol) equilibrated in the presence of SPS bioMIPs (hot-wash, 10 pM), was considered as maximum binding. Then, each competitor molecule was added at a concentration of $3 \times K_D$ and incubated for 1 h before reading. The addition of IL-6 produced a clear displacement effect, suggesting efficient competition between the full IL-6 protein and its tagged C-terminal epitope. In contrast, the addition of other proinflammatory interleukins, such as IL-1β, IL-8 and IL-11 did not result in a significant displacement, suggesting the IL-6 GelMA bioMIPs were selective for the targeted cytokine. Selectivity was confirmed also when the pro-regenerative cytokines, such as IL-4 and IL-13 were used as competitors and at last was maintained when the competitors were abundant serum proteins, such as human serum albumin (HSA) and human serum transferrin (HTR).

2.5. Ex-vivo scavenging of IL-6 in serum samples

Finally, the SPS bioMIPs were tested for their ability to scavenge IL-6 in commercial human serum samples, so as to determine their potential in subsiding inflammation-stimulating molecules under real physiological conditions and in a complex biological sample. Preliminary investigations were conducted to assess the binding behavior in serum of control nanoparticles, in the form of non-imprinted GelMA NPs (SI Fig. 11.1, grey squares) and to compare it with the effects of SPS bioMIPs (SI Fig. 11.1, red circles) and of bioMIPs made in-solution (Fig. 11.1, open hexagons). Results showed control NPs exhibiting no detectable change in fluorescence, indicating negligible binding under the tested conditions. In contrast, SPS bioMIPs (red circles) produced pronounced fluorescence responses at picogram concentrations, whereas bioMIPs synthesized in solution (open hexagons) generated measurable signals at nanogram levels, highlighting their comparatively lower sensitivity. Next, commercial serum samples were spiked with a known concentration of IL-6 (200 pg/mL). A fixed volume of spiked serum (100 μL) was incubated with 10 ng of hot-wash harvested SPS bioMIPs, or cold-wash GelMA NPs (80 ng), or bioMIPs prepared by in-solution synthesis (3 μg), or GelMA CTRL NPs (3 μg). After the incubation (30 min), the levels of IL-6 were tested in all samples. The quantity of sequestered IL-6 was estimated and normalized for the quantity of added GelMA NPs.

Fig. 9 summarizes the IL-6 uptake performance of GelMA-based bioMIPs synthesized *via* the two different routes. BioMIPs prepared by in-solution imprinting exhibited an IL-6 uptake from commercial serum of 26 ± 3 pg/μg (white bar), while non-imprinted GelMA nanoparticles (CTRL) showed negligible binding (1 ± 0.5 pg/μg, grey bar). BioMIPs recovered by the cold-wash step displayed a modest improvement (4 ± 1 pg/μg, blue bar). Strikingly, SPS bioMIPs recovered from the hot-wash step demonstrated an exceptional ability to sequester IL-6, reaching 1178 ± 101 pg/μg (red bar). This, in agreement with in serum isotherms (SI Fig. 11.1), represents a ~45-fold enhancement in the IL-6 cytokine capture compared to the in-solution–synthesized

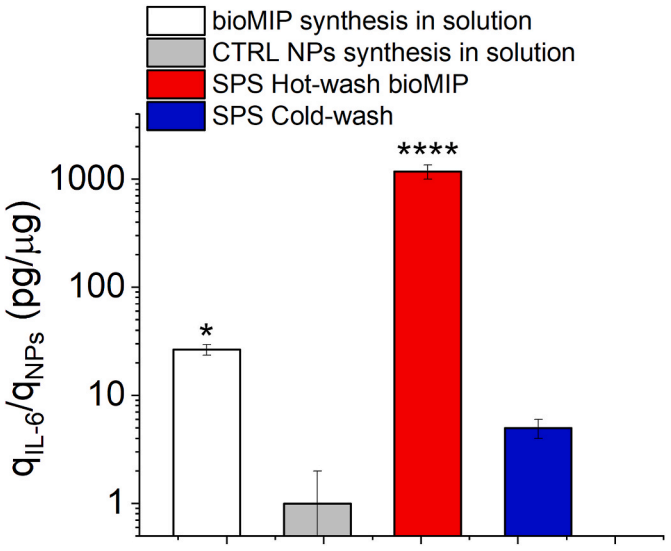

Fig. 9. IL-6 uptake from commercial serum by GelMA nanoaggregates prepared using different synthesis methods. Bar graph showing specific IL-6 uptake (pg/μg of NPs) from commercial serum by GelMA nanoaggregates prepared via in-solution synthesis (26 pg/μg, white bar), in solution synthesized GelMA CTRL NPs (1 pg/μg, grey bar), SPS cold-wash particles (4 pg/μg, blue bar), and SPS bioMIPs obtained after hot-wash (1178 pg/μg, red bar), with the SPS bioMIPs exhibiting the highest IL-6 sequestration capacity among all conditions tested. Statistical comparisons were performed against CTRL NPs using Dunnett's multiple comparisons test following one-way ANOVA: *$p < 0.05$; **$p < 0.01$; ***$p < 0.001$; ****$p < 0.0001$. (For interpretation of the references to colour in this figure legend, the reader is referred to the Web version of this article.)

bioMIPs, qualifying SPS bioMIPs as template-free high-quality scavengers of IL-6 and underscoring the superior imprinting precision and affinity achieved through the solid-phase synthesis process.

To further quantify the effectiveness of the molecular imprinting process in creating selective binding sites for the target molecule, the imprinting factor (IF) was estimated. The IF is defined as the ratio of target analyte bound by an imprinted material relative to that bound by a non-imprinted control, and it serves as a quantitative metric of imprinting efficiency by reflecting the enhancement in binding performance. As such, it provides a direct measure of the specificity, affinity, and overall quality of the imprinted recognition sites. From Fig. 9, hot-wash SPS bioMIPs exhibit an IF ~294 relative to cold-wash NPs, whereas bioMIPs prepared via in-solution phase showed an IF ~26 with respect to CTRL NPs, highlighting the significant improvement of the SPS approach.

Then, the binding capacity of the SPS bioMIPs was compared to that reported for polyacrylamide-based molecularly imprinted nanogels synthesized by the SPS strategy. As an example, polyacrylamide-based molecularly imprinted nanogels selective for tumour necrosis factor-α (TNF-α) were earlier reported to scavenge the 100% of TNF-α (i.e. 1136 pg/mL) from cell supernatants at the polymer concentration of 100 μg/mL, thus corresponding to about 1 ng/100 μg [49]. In contrast, GelMA-based SPS bioMIPs incubated in human serum demonstrated a scavenge performance towards their target (IL-6) corresponding to about 1 ng/μg, while composed of a natural, biocompatible protein-based polymer scaffold. Even with the preliminary character of these experiments, the SPS bioMIPs removal of the targeted cytokine from serum underlines robust recognition under physiologically relevant conditions and opens the way for SPS bioMIPs to mitigate inflammation. Collectively, these findings suggest that the SPS approach enables the fabrication of highly efficient, naturally derived bioMIPs with important recognition capability in physiologically relevant environments, marking a significant advancement toward scalable, safe, and selective cytokine scavengers for biomedical applications.

2.6. Batch-to-batch reproducibility, storage and reusability of template

The SPS bioMIPs demonstrated remarkable batch-to-batch reproducibility, as evidenced by their consistent hydrodynamic size distribution in number measured by DLS (Fig. 10A). Functional reproducibility was further confirmed through binding assays using TAMRA-IL-6Cterm peptide (8 pmol/well), where bioMIPs (10 ng) obtained from three independent syntheses on three different solid supports, exhibited highly comparable binding profiles following hot-wash purification (Fig. 10B). In addition, storage stability was assessed by comparing freshly prepared and 45-day-stored (4 °C) hot-wash bioMIPs from the same batch, which showed no significant differences in binding performance (Fig. 10C). The reusability of the solid support was also investigated through multiple synthesis cycles performed on the glass beads covalently functionalized with IL-6Cterm. As shown in Fig. 10D,

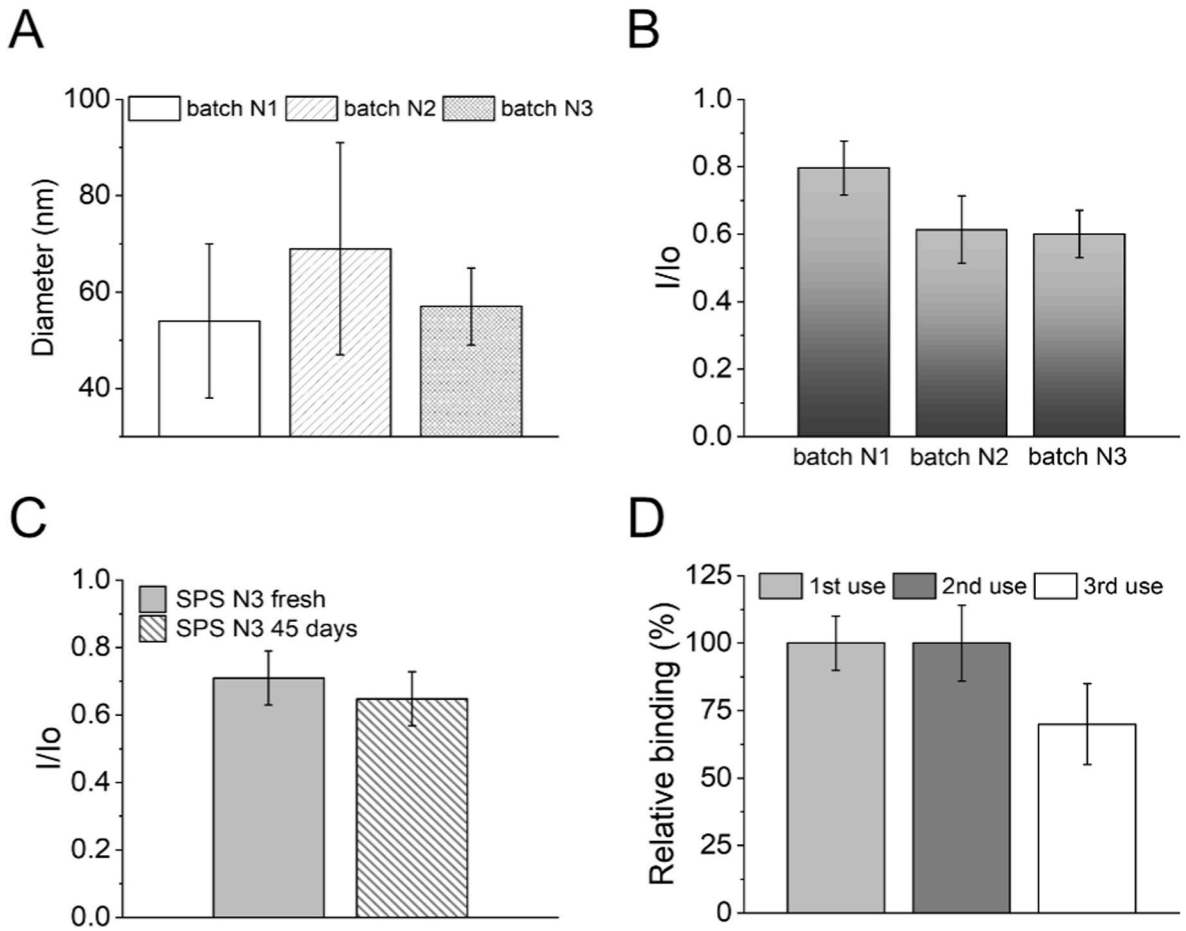

Fig. 10. Reproducibility, stability, and solid-support reusability of SPS bioMIPs. (A) Dynamic light scattering (DLS) analysis showing comparable size distributions for bioMIPs obtained from independent synthesis batches (arbitrarily numbered 1, 2, 3). (B) The binding performance of hot-wash bioMIPs (10 ng) produced from three separate syntheses toward TAMRA-IL-6Cterm (5 pmol/well), demonstrating consistent binding behavior across batches. (C) Comparison of binding activity of hot-wash bioMIPs (10 ng/well) from the same batch tested immediately after synthesis and after 45 days of storage at 4 °C, indicating preserved binding capability over time. (D) Evaluation of solid-support reusability: SPS bioMIPs synthesized on solid supports (GB) covalently functionalized with IL-6Cterm retain comparable binding efficiency across two consecutive synthesis cycles, whereas a third cycle results in reduced binding performance.

bioMIPs produced using the same support for two consecutive cycles retained equivalent binding efficiency, whereas a third cycle resulted in a ~30% decrease in binding, indicating partial loss of template integrity or surface functionality over repeated use.

3. Conclusions

This study is the first to investigate conditions for producing homogeneous, target-selective protein-derived nano-sized molecular traps, specifically the IL-6 selective GelMA bioMIPs, using solid-phase synthesis. Synthetic conditions were devised by real-time monitoring of the GelMA nucleation process on a plasmonic surface, functionalized with target templates acting as anchored template-baits. Among the tested surfaces, the best bioMIP nucleation occurred on PEG_{12}-IL-6Cterm, a surface characterized by template-baits protruding into the solvent as antennas, making it accessible to GelMA for nucleation. Sparser baits (12% coverage of the surface) provided superior nucleation conditions with respect to higher bait's densities. The use of quasi-limiting GelMA quantities (100 ng/surface) promoted the formation of homogeneous and monomodal bioMIPs.

Next, the SPS for bioMIPs concept was implemented as a miniaturized planar reactor filled with template-immobilized GBs was tested for the production of IL-6-selective SPS bioMIPs. Planar design was preferred, with respect to column-designed vessels [22–24], to limit UV scattering and meanwhile maximize the radiant energy on the GBs, as the GelMA bioMIPs are stabilized by crosslinking *via* photo-polymerization. The proof-of-concept reactor showed a synthetic yield of 19% and a quantity of harvested GelMA bioMIPs of about 200 ng per cycle. The reactor process demonstrated a straightforward and effective fabrication route for GelMA-derived meta-biomaterials, and, to the best of our knowledge, represents the first report of SPS-based bioMIP production.

Challenged for selective recognition of the template, SPS GelMA bioMIPs showed a picomolar dissociation constant for the template (K_{Dapp} 21.65 ± 4.22 pM) supporting for a strong affinity for their target. SPS bioMIPs exhibited an apparent 753 times lower dissociation constant with respect to their in-solution synthesized counterparts, with the improved affinity reflecting the design of the solid-phase synthesis as a process that ensures nucleation of each individual particle around at least one template bait. Selectivity for the targeted cytokine was confirmed both in buffer solution and serum samples, highlighting the scavenging potential of these IL-6 SPS bioMIPs.

The present reactor design yields high-quality binders and clearly demonstrates the successful imprinting process with protein-based materials (i.e. GelMA), resulting in binding affinities comparable to those obtained with non-natural imprinted-materials (i.e. polyacrylamides) [50,51], and highlighting the competitive performance of solid-phase imprinting applied to biopolymer-derived materials. Scaling up bioMIP production to gram-scale quantities, while ensuring efficient recovery, requires careful evaluation of reactor design. This includes the implementation of tailored systems based on dispersed-phase imprinting strategies, where template-functionalized magnetic beads act as mobile solid phases. In such configurations, the isolation of imprinted materials can be achieved through magnetic separation (pulldown), followed by solvent exchange for purification [52].

Overall, our findings establish a robust, controlled, and reproducible synthesis protocol for bioMIPs within an integrated reactor platform, and, importantly, provide a concrete pathway for transitioning from laboratory-scale synthesis to scalable and potentially continuous bioMIP manufacturing. The synergy between an exceptionally facile fabrication process and the biocompatibility, biodegradability, and non-toxicity of natural polymers positions these materials as strong candidates for developing meta-biomaterials for healthcare and beyond, opening possibilities in systemic administration and *in vivo* translation, as well as serving in the design of intelligent meta-biomaterials for tissue engineering and single-cell patterning platforms.

4. Materials and methods

4.1. Chemicals and materials

Glass beads G8893, Tris free base, Phosphate buffer saline (PBS) P3813 powder pH 7.4, R,S-lipoic acid (LA), Lithium phenyl-2,4,6-trimethylbenzoylphosphinate (LAP), and Human male serum were from Sigma Aldrich, Milan, Italy. Gelatin type B was from Glentham Life Science, Corsham, UK. Sulfuric acid, hydrogen peroxide, and Dimethylformamide (DMF) were from Honeywell Fluka, Buchs, Swiss. Interleukin-6 (IL-6) and Interleukin-1beta (IL-1β) were from Thermo Fisher, Waltham, MA US. Silane-PEG-OH and Silane-PEG-DBCO MW 1000 Da, Nanosoftpolymers, Winston-Salem, NC, US. Peptides, EFLQSSLRALRQM, azidacetic acid-EFLQSSLRALRQM peptide (N_3-IL-6Cterm), 5-Carboxytetramethylrhodamine-EFLQSSLRALRQM (TAMRA-IL-6Cterm) were from OligoMaker ApS, Frederiksberg, Denmark. Quantikine QuicKit IL-6 ELISA was from Bio-Techne, Minneapolis, MN, US. Near-UV transparent polymeric chambers with a diameter of 3.5 cm and 96 black flat-bottom wells were from Corning Inc. (Corning, NY, US).

4.2. Preparation of the GelMA

Gelatin methacryloyl (GelMA) was prepared according to the protocol reported by Ren, T. et al. [53], with slight modifications. Briefly, a 10% w/V gelatin type B (powder from porcine skin by Glenham Life Science) solution was prepared in PBS pre-heated at 50 °C. The solution was left under stirring for 1 h and then 8 mL of methacrylic anhydride (8.28 g, 53.7 mmol) were added dropwise. The reaction solution was left under stirring at 50° for 2.5 h and then transferred into a 3.5 kDa MWCO dialysis bag and dialyzed against DI water at 40-45 °C for 7 to 15 days until complete removal of unreacted species. The solution was then freeze-dried and lyophilized GelMA was stored at −20 °C until use.

4.3. In-solution synthesis of bioMIPs and control GelMA NPs

To prepare bioMIPs, GelMA concentration was adjusted to 0.3% in 5 mM of phosphate buffer (PB) pH 7.0 buffer and heated at 80 °C for 10 min, then at 50 °C for 10 min and finally temperature was set at 37 °C. A quantity of 6 nmol of the print molecule IL-6Cterm template peptide of sequence EFLQSSLRALRQM (OligoMaker ApS, Frederiksberg, Denmark). The final volume was 2 mL. The photoinitiator Lithium phenyl-2,4,6-trimethylbenzoylphosphinate (LAP, Sigma-Aldrich, Darmstadt, Germany) was added at the final concentration of 0.02% w/v, and photo-polymerized for 2 min under UV light $\lambda = 365$ nm (radiant power 1.2 W, Intelligent LED Solutions, model ILH-XT01-S365-SC211-WIR200, US) [3]. At the end of the polymerization process, the template was removed by the addition of Trizma free base to the NPs suspension to reach a pH of 10.5 for 1 h. Samples were heated in the heating chamber at 45 °C for 30 min under stirring to perform the thermal wash. Dialysis was performed in 300 mL of water for 1 h and then in 3.5 L of water overnight under stirring, followed by further dialysis in 3.5 L of water for 3 h repeated twice the following day. Samples were freeze-dried for storage. When used immediately, samples were dialyzed in PBS for 3 h. As controls, GelMA NPs were synthesized in a same manner, but in the absence of the IL-6Cterm template.

4.4. Preparation of solvated GelMA building blocks

GelMA concentration was adjusted to 3000, 500, and 1 μg/mL in MilliQ water. To ensure full solvation of GelMA, the solution was heated at 80 °C for 10 min, then at 50 °C for 20 min.

4.5. Preparation on the SPR real-time monitoring device

Real-time monitoring of GelMA nucleation was performed by means

of a portable surface plasmon resonance (SPR) platform, equipped with a gold coated (~60 nm thickness) D-shaped polymer optical fibers (Moresense s.r.l., Milan, Italy) functionalized with the template peptide (IL-6Cterm).

The gold surfaces were cleaned by oxygen plasma treatment (60s, 90 W). A first surface condition for nucleation (LA-IL-6Cterm) was based on a lipoic acid (240 μM) self-assembled monolayer (SAM), formed by incubating the gold surface with 100 μL of solution overnight at RT. Alternatively, the SAM was formed using a 20:1 mol:mol ratio of thiol-dPEG$_4$-OH:thiol-dPEG$_{12}$-COOH in a final volume of 100 μL, incubated overnight at RT (PEG-IL-6Cterm).

The day after, both surfaces were thoroughly rinsed with Milli-Q water (4× washes), carboxyl groups were activated by incubation with 100 μL of a solution containing EDC (25 mM) and NHS (10 mM) in 5 mM MES buffer (pH 5.5) for 20 min at RT. The surfaces were then rinsed with Milli-Q water and incubated with 100 μM of the peptide IL-6Cterm in 10 mM PB buffer for 20 min at RT. Unreacted sites were blocked with 5 mM glycine for 10 min at RT. Prior to use SPR surfaces were thoroughly rinsed with Milli-Q water.

4.6. Real-time monitoring of GelMA nucleation

For the real-time nucleation experiments, a volume of 100 μL of GelMA solution at the concentrations of 3000, 500, 1 μg/mL, which corresponds to 300 μg, 50 μg and 100 ng, was placed onto the functionalized SPR surface (LA-IL-6Cterm or PEG-IL-6Cterm) and incubated up to 60 min at RT. The plasmonic signal was monitored every 5 min throughout the incubation. After 60 min, the solution was removed and collected in an Eppendorf tube for further analysis. Subsequently, a volume of 100 μL of LAP (10 μg/mL) solution was rapidly added, according to Ref. [3], and photopolymerization was initiated by switching on a LED (λ 365 nm) light source for 2 min. The SPR surface was then washed twice with 100 μL of cold MilliQ water (stored at 4 °C) by pipetting to remove non imprinted GelMA nanoparticles. To recover the high affinity GelMA bioMIPs, 150 μL of MilliQ water were added onto the SPR surface and incubated for 10 min at 43 °C. SPR chip surface recovery was performed by washes with Tris free base (20 mM, pH 10) heated at 43 °C by pipetting, to ensure the removal of any residual from the surface. The recovery was ensured by the plasmonic signal. At each step of the procedure, the wavelength shift was measured by SPR, and all collected volumes were stored in Eppendorf tubes.

4.7. Setup of the solid-phase synthesis reactor

As a reactor near-UV transparent polymeric chambers with a diameter of 3.5 cm were used. Prior to fill the chambers, glass beads (GBs) were functionalized with the template, in a reaction modified from Ref. [25]. Glass Beads (GBs, G8893, Sigma Aldrich) were washed in piranha solution (3:1 v/v of H_2SO_4 97% and H_2O_2 30% w/w) for 1 h at 90 °C, then rinsed multiple times with dH_2O, filtered, and vacuum dried. Solutions of 100 μg/mL of Silane-PEG-OH and Silane-PEG-DBCO (MW 1000 Da, Nanosoftpolymers, US) at different ratios (1:1, 10:1, 20:1 v/v) were prepared in anhydrous DMF. A 1 g of washed GBs was incubated in 400 μL of Silane-PEG-OH:Silane-PEG-DBCO at 90 °C for 2 h, rinsed with DMF and dH_2O, filtered, and dried under vacuum. Next, 500 mg of silanized GBs were incubated in a vial with 500 μL of a 30 μM solution of N_3-EFLQSSLRALRQM peptide in 25 mM PB pH 7.4 at RT for 3 h. The vial was then centrifuged and the peptide solution removed. IL-6Cterm-GBs were washed 2 times with PB and 4 times with dH_2O.

4.8. Solid-phase synthesis of GelMA bioMIPs

The quantity of GBs to be deposited in each reactor plate was calculated from the volume occupied by a single GB, $V_{GB} = 1.13 \times 10^{-7} cm^3$. Being the density of the GBs $\rho_{GB} = 2.5\ g/cm^3$, the mass of a GB was equal to $m_{GB} = 2.83 \times 10^{-7} g$. Being the reactor plate size of diameter 35 mm and the number of GBs accommodated in a plate equal to 3.35×10^5, the mass of GBs in a reactor plate was 94.6 *mg*. One hundred mg of IL-6Cterm-GBs was deposited in each reactor plate of a 6 polymeric chambers plate. A 2.0 μg/mL GelMA solution in Milli-Q water was prepared according to Section "*Preparation of solvated GelMA building blocks*". A 600 ng/mL LAP solution in Milli-Q water was prepared and filtered with a 0.45 μm filter. IL-6Cterm-GBs were incubated with 1 mL GelMA solution for 60 min at room temperature, then the solution was removed and plates were filled with 1 mL LAP solution and exposed to $\lambda = 365$ nm UV light (SpotLED Curing Equipment, Photo Electronics srl, 15 W, 43.3 mW/cm^2) for 2 min. Next, the solution was withdrawn and IL-6Cterm-GBs were washed twice for 2.5 min with 1 mL of 4 °C Milli-Q water (cold-wash). IL-6Cterm-GBs were next washed with 1 mL of 65 °C Milli-Q water for 10 min in oven under mild agitation (hot-wash). Each fraction was collected and used for further analysis.

4.9. Dynamic light scattering (DLS)

Size distribution and polydispersity index (PDI) were determined by Dynamic Light Scattering (DLS) using a Zetasizer Nano ZEN3600 (Malvern Instruments Ltd, Worcestershire, UK) equipped with a 633 nm He-Ne laser. Collected fractions were concentrated 20 times with Microcon 30 kDa M W.C.O. filters (Millipore, MI, US) at 7000 rpm prior to measurements. The material refractive index (RI) was 1.490 and the absorption value 0.01; the dispersant RI was 1.332 for, the viscosity was 0.89 cP as reported by the Zetasizer v.6.32 software (Malvern Instruments Ltd, Worcestershire, UK). The temperature was set at 273 K and a detection angle of 173° was used. Measurements were in triplicate.

4.10. Microscopy characterization

Atomic Force Microscopy: Topographical reconstruction of the POF-SPR surfaces was carried out using an NT-MDT NTEGRA Prima microscope equipped with a universal SPM head operated in semi-contact mode. Silicon cantilevers (NSG-11, NT-MDT; tip radius ~10 nm; resonance frequency 181 kHz) were employed. For each sample, 1 × 1 μm topography maps (1024 × 1024 pixels) were acquired after (i) lipoic acid + peptide functionalization, (ii) bioMIPs nucleation, and (iii) bioMIPs after washing. The datasets were subsequently processed and visualized using Gwyddion analysis software [54].

Electron Microscopy: Transmission Electron Microscopy (TEM) analysis was performed with using a TALOS F200S (ThermoFisher, USA) with a maximum acceleration voltage of 200 kV. Scanning electron microscopy (SEM) images of GelMA nanotraps were obtained using a Supra 40 (Zeiss, Germany) Field-Emission Scanning Electron Microscope. Images were acquired in secondary electron at 3 kV. The as-synthesized nanotrap suspension was deposited either onto monocrystalline gold-coated silicon chips (120 nm thickness) or onto Formvar/carbon-supported copper grids (200 mesh), and subsequently dried prior to imaging by SEM and TEM, respectively. The size distribution of the particles was estimated manually by measuring the diameter of about 500 particles on 3 calibrated images (10,000 × magnification) using ImageJ software.

4.11. Fluorescence binding assay

Fractions of GelMA bioMIPs were concentrated using Microcon 50 kDa M W.C.O. filters (Millipore, MI, US) at 7000 rpm prior to measurements. GelMA bioMIPs were filtered onto a 0.45 μm microfuge filter, then diluted in PBS 10 mM pH 7.4 to 13 or 26 ng/well. A fixed quantity of 2.5 pmol/well of peptide IL-6Cterm-TAMRA in PBS 10 mM pH 7.4 was used to test the binding. Measurements were performed in triplicate on 96 Flat Bottom Black Polystyrene microtiter plates (ThermoScientific, Germany) using a Tecan Infinite 200 Pro M Plex Microplate

Reader – AV (Boston Industries, Boston, MA). Wells were loaded with a final volume of 100 μL, of in-solution synthesized GelMA bioMIPs (50 and 500 ng), control non-imprinted GelMA NPs (20 ng), or solid phase synthesis fractions: cold-wash 26 ng, hot-wash 13 ng. Incubated for a minimum of 10 min and read up to 180 min. The excitation was at the $\lambda_{exc} = 522$ nm, and emission was recorded in the range 528-640 nm. Maximum λ_{em} was at 586 nm.

Data were analyzed using a one-way analysis of variance (ANOVA) with a normal (Gaussian) distribution assumption. The analysis included six experimental groups (A–F): GelMA CTRL, TAMRA-IL-6Cterm, bioMIP 50 ng, bioMIP 500 ng, Cold wash, and Hot wash, with three replicates per group ($n = 3$), for a total of 18 observations. Homogeneity of variances was assessed using the Brown-Forsythe test prior to ANOVA. Following the overall ANOVA, pairwise comparisons against the control group (GelMA CTRL) were performed using Dunnett's multiple comparisons test, with a family-wise significance threshold set at $\alpha = 0.05$. Adjusted p-values are reported for each comparison. All statistical analyses were performed using GraphPad Prism.

4.12. Binding isotherm in fluorescence of GelMA bioMIP hot-wash

GelMA bioMIPs hot-wash fraction was concentrated using Microcon 50 kDa M W.C.O. filters (Millipore MI, US) at 7000 rpm prior to measurements, filtered onto a 0.45 μm microfuge filter, and diluted in PBS 10 mM pH 7.4 in the range from 1 pM to 5 nM. A fixed quantity of 5 pmol/well of peptide IL-6Cterm-TAMRA in PBS 10 mM pH 7.4 was used for the binding isotherm. As a control, GelMA CTRL non imprinted NPas were used at the same concentrations. Measurements were performed in triplicate on 96 Flat Bottom Black Polystyrene microtiter plates (ThermoScientific, Germany) using a Tecan Infinite 200 Pro M Plex Microplate Reader – AV (Boston Industries, Boston, MA). Wells were loaded with a final volume of 100 μL, incubated for a minimum of 10 min and read up to 180 min. The excitation was at the $\lambda_{exc} = 522$ nm, and emission was recorded in the range 528-640 nm. Maximum λ_{em} was at 586 nm.

4.13. Competitive binding tests

The fraction GelMA bioMIPs hot-wash was concentrated using Microcon 50 kDa M W.C.O. filters (Millipore MI, US) at 7000 rpm prior to measurements and filtered onto a 0.45 μm microfuge filter. Then GelMA bioMIPs were incubated at the fixed concentration of 10 pM in PBS 10 mM pH 7.4 in the presence of 2.5 pmol/well of peptide IL-6Cterm-TAMRA; or with 2.5 pmol/well of peptide IL-6Cterm-TAMRA and a concentration of competitor protein (IL-6, IL1, Il-4, IL8, IL-11, IL-13, human serum albumin, human serum transferrin) equal to 3 times the value of the K_D of the complex SPS bioMIP hot-wash and peptide IL-6Cterm-TAMRA. Measurements were performed in triplicate on 96 Flat Bottom Black Polystyrene microtiter plates (ThermoScientific, Germany) using a Tecan Infinite 200 Pro M Plex Microplate Reader – AV (Boston Industries, Boston, MA). Wells were loaded with a final volume of 100 μL, incubated for a minimum of 10 min and read up to 180 min. The excitation was at the $\lambda_{exc} = 522$ nm, and emission was recorded in the range 528-640 nm. Maximum λ_{em} was at 586 nm. The fluorescence emission of 2.5 pmol/well of peptide IL-6Cterm-TAMRA was considered I_o.

4.14. Ex vivo IL-6 scavenging

IL-6 levels were quantified using a commercial Quantikine QuicKit ELISA (Bio-Techne/R&D Systems, Minneapolis, MN, US) according to the manufacturer's instructions. All reagents, including the pre-coated microplate, human IL-6 standard, human IL-6 capture and detection antibodies, diluent and wash buffer, colour reagents and stop solution, were supplied with the kit. The calibration curve was obtained using the human IL-6 standard provided by the kit, with concentrations ranging from 800 to 12.5 pg/mL. Sample measurements were performed using commercial human serum (Sigma-Merck) as the sample matrix. Control samples included commercial human serum and commercial human serum spiked with IL-6 to a final concentration of 200 pg/mL. Experimental samples consisted of commercial human serum diluted 1:1, spiked with IL-6 (100 pg/mL final concentration) and incubated with GelMA NPs for 30 min prior to the addition of the antibody cocktail and subsequent analysis. All standards and samples were measured in triplicate. The colorimetric signal was measured at 655 nm before addition of the stop solution, and after the addition at 450 nm, using an Epoch microplate reader (BioTek Instruments, Winooski, VT, US). The IL-6 concentrations were determined from the standard curve: y (OD@655 nm) = 0.0017 × (pg/mL of IL-6) – 0.0058, $R^2 = 0.9956$ and expressed as pg/mL. Data were analyzed using a one-way analysis of variance (ANOVA) with a normal (Gaussian) distribution assumption. The analysis included four experimental groups (A–D): GelMA CTRL, bioMIP, Cold wash, and Hot wash, with three replicates per group ($n = 3$), for a total of 12 observations. Homogeneity of variances was assessed using the Brown-Forsythe test prior to ANOVA. Following the overall ANOVA, pairwise comparisons against the control group (GelMA CTRL NPs) were performed using Dunnett's multiple comparisons test, with a family-wise significance threshold set at $\alpha = 0.05$. Adjusted p-values are reported for each comparison. All statistical analyses were performed using GraphPad Prism.

4.15. Batch to batch repeatability; reusability; storage

Batch-to-batch reproducibility of SPS bioMIPs was evaluated by comparing $n = 3$ independently synthesized batches under identical experimental conditions. Fluorescent binding assays were performed as follows: GelMA bioMIPs hot-wash fractions were first concentrated using Microcon 50 kDa molecular weight cut-off filters (Millipore, MI, USA) at 7000 rpm. The samples were subsequently filtered through 0.45 μm microfuge filters. A fixed amount of 5 pmol per well of IL-6Cterm-TAMRA peptide in PBS (10 mM, pH 7.4) was used as the fluorescent probe and a fixed quantity of bioMIPs (10 ng) was used. Measurements were performed in triplicate in 96-well flat-bottom black polystyrene microtiter plates (Thermo Scientific, Germany), with a final volume of 100 μL per well. Samples were incubated for at least 10 min and fluorescence was monitored up to 60 min using a Tecan Infinite 200 PRO M Plex microplate reader (Tecan Group Ltd., Männedorf, Switzerland). Excitation was set at $\lambda_{exc} = 522$ nm, and emission spectra were recorded between 528 and 640 nm, with maximum emission observed at 586 nm. Likewise, to assess storage stability, bioMIP samples were stored in PBS (10 mM, pH 7.4) at 4 °C temperature for up to 45 days. Binding performance was evaluated over time using the same fluorescence assay conditions and compared to freshly prepared samples. For the reusability of the solid-phase, this was used to prepare bioMIPs for $n = 3$ consecutive cycles. After each cycle, particles were recovered, concentrated as above and their binding capacity was assessed using the above protocol. Binding responses across cycles were compared to evaluate performances.

Funding sources

A.M. Bossi and D. Maniglio were funded by European Union – NextGenerationEU, component M4C2, investment 1.1, project PRIN2022 'nanoTRiCKS': tailor-made biopolymeric nanotraps for cytokines' storm suppression", project code 20228AYRJE. Additionally, A. M. Bossi and D. Maniglio received funding from PRIN PNRR "BIAS": Biomips ImmunomodulAting Scaffolds for tissue engineering, project code: P2022HLS3M.

CRediT authorship contribution statement

Devid Maniglio: Conceptualization, Data curation, Formal analysis,

Funding acquisition, Investigation, Methodology, Project administration, Supervision, Validation, Visualization, Writing – original draft, Writing – review & editing. **Alice Marinangeli:** Conceptualization, Data curation, Investigation, Methodology, Validation, Visualization, Writing – original draft, Writing – review & editing. **Daniel Moranduzzo:** Data curation, Formal analysis, Investigation, Methodology, Validation, Writing – original draft. **Giacomo Canevari:** Conceptualization, Data curation, Formal analysis, Methodology, Software, Supervision, Visualization, Writing – original draft. **Mauro Bonafini:** Conceptualization, Data curation, Software, Validation, Visualization, Writing – original draft. **Chiara Stranieri:** Data curation, Investigation, Methodology, Validation, Writing – original draft. **Edoardo Di Leo:** Data curation, Investigation, Methodology, Writing – original draft. **Giorgio Speranza:** Data curation, Investigation, Methodology, Visualization, Writing – original draft. **Giandomenico Orlandi:** Conceptualization, Methodology, Resources, Software, Supervision, Validation, Writing – original draft. **Anna Maria Fratta Pasini:** Data curation, Formal analysis, Investigation, Methodology, Supervision, Writing – original draft. **Alessandra Maria Bossi:** Conceptualization, Data curation, Funding acquisition, Investigation, Methodology, Project administration, Supervision, Validation, Visualization, Writing – original draft, Writing – review & editing.

Declaration of competing interest

The authors declare that they have no known competing financial interests or personal relationships that could have appeared to influence the work reported in this paper.

Acknowledgements

A.M. Bossi thanks the Centro Piattaforme Tecnologiche (CPT), University of Verona, for the use of the DLS, and Zetasizer. A.M. Bossi and D. Maniglio thanks funding by European Union – NextGenerationEU, component M4C2, investment 1.1, project PRIN2022 ‘nanoTRiCKS’: tailor-made biopolymeric nanotraps for cytokines' storm suppression”, project code 20228AYRJE. Additionally, A.M. Bossi and D.Maniglio received funding from PRIN PNRR “BIAS”: Biomips ImmunomodulAting Scaffolds for tissue engineering, project code: P2022HLS3M.

Appendix A. Supplementary data

Supplementary data to this article can be found online at https://doi.org/10.1016/j.mtbio.2026.103094.

Data availability

Data will be made available on request.

References

[1] A.M. Bossi, A. Bucciarelli, D. Maniglio, Molecularly imprinted silk fibroin nanoparticles, ACS Appl. Mater. Interfaces 13 (2021), https://doi.org/10.1021/acsami.1c05405.
[2] D. Maniglio, F. Agostinacchio, A.M. Bossi, Silk fibroin molecularly imprinted nanoparticles as biocompatible molecular nanotraps: molecular recognition ties the knot with biomaterials. The bioMIP's labeling and degradation, MRS Adv. 8 (2023), https://doi.org/10.1557/s43580-023-00507-3.
[3] A.M. Bossi, S. Casella, C. Stranieri, A. Marinangeli, A. Bucciarelli, A.M. Fratta Pasini, D. Maniglio, Protein-based molecular imprinting: gelatin nanotraps for interleukin-6 sequestration in inflammation cell models, Trends Biotechnol. 43 (2025), https://doi.org/10.1016/j.tibtech.2025.02.002.
[4] R. Arshady, K. Mosbach, Synthesis of substrate-selective polymers by host-guest polymerization, Makromol. Chem. 182 (1981) 687–692, https://doi.org/10.1002/macp.1981.021820240.
[5] G. Wulff, J. Liu, Design of biomimetic catalysts by molecular imprinting in synthetic polymers: the role of transition state stabilization, Acc. Chem. Res. 45 (2012), https://doi.org/10.1021/ar200146m.
[6] J.J. Belbruno, Molecularly imprinted polymers, Chem. Rev. (2019), https://doi.org/10.1021/acs.chemrev.8b00171.
[7] Y. Wan, C. Liu, S. Wang, K. Ye, Y. Ding, S. Li, X. Cheng, Z. Liu, Z. Xu, Molecularly imprinted framework materials: design, synthesis, applications, and perspectives, Coord. Chem. Rev. 547 (2026), https://doi.org/10.1016/j.ccr.2025.217117.
[8] T. Cowen, D. Maniglio, A.M. Bossi, Molecular imprinting using biopolymers as building blocks: sustainable and biocompatible metamaterials for smart recognition and selective biointerfaces, TrAC, Trends Anal. Chem. 193 (2025), https://doi.org/10.1016/j.trac.2025.118422.
[9] J. Fang, A. Mehlich, N. Koga, J. Huang, R. Koga, X. Gao, C. Hu, C. Jin, M. Rief, J. Kast, D. Baker, H. Li, Forced protein unfolding leads to highly elastic and tough protein hydrogels, Nat. Commun. 4 (2013), https://doi.org/10.1038/ncomms3974.
[10] B.v. Slaughter, S.S. Khurshid, O.Z. Fisher, A. Khademhosseini, N.A. Peppas, Hydrogels in regenerative medicine, Adv. Mater. 21 (2009), https://doi.org/10.1002/adma.200802106.
[11] D. Caballero, C.M. Abreu, A.C. Lima, N.N. Neves, R.L. Reis, S.C. Kundu, Precision biomaterials in cancer theranostics and modelling, Biomaterials 280 (2022), https://doi.org/10.1016/j.biomaterials.2021.121299.
[12] K. Yue, G. Trujillo-de Santiago, M.M. Alvarez, A. Tamayol, N. Annabi, A. Khademhosseini, Synthesis, properties, and biomedical applications of gelatin methacryloyl (GelMA) hydrogels, Biomaterials 73 (2015), https://doi.org/10.1016/j.biomaterials.2015.08.045.
[13] G.H. Altman, F. Diaz, C. Jakuba, T. Calabro, R.L. Horan, J. Chen, H. Lu, J. Richmond, D.L. Kaplan, Silk-based biomaterials, Biomaterials 24 (2003), https://doi.org/10.1016/S0142-9612(02)00353-8.
[14] R.H. Myers, A. Khuri, W.H. Carter, Response surface methodology: 1966-1988, Technometrics 31 (1989), https://doi.org/10.1080/00401706.1989.10488509.
[15] Y. Hoshino, T. Kodama, Y. Okahata, K.J. Shea, Peptide imprinted polymer nanoparticles: a plastic antibody, J. Am. Chem. Soc. 130 (2008) 15242–15243, https://doi.org/10.1021/ja8062875.
[16] P.L. McGeer, E.G. McGeer, Inflammation and the degenerative diseases of aging, Ann. N. Y. Acad. Sci. (2004), https://doi.org/10.1196/annals.1332.007.
[17] L. Ferrucci, E. Fabbri, Inflammageing: chronic inflammation in ageing, cardiovascular disease, and frailty, Nat. Rev. Cardiol. 15 (2018), https://doi.org/10.1038/s41569-018-0064-2.
[18] B.J. Laird, D.C. McMillan, P. Fayers, K. Fearon, S. Kaasa, M.T. Fallon, P. Klepstad, The systemic inflammatory response and its relationship to pain and other symptoms in advanced cancer, Oncologist 18 (2013), https://doi.org/10.1634/theoncologist.2013-0120.
[19] I.M. Rea, D.S. Gibson, V. McGilligan, S.E. McNerlan, H. Denis Alexander, O.A. Ross, Age and age-related diseases: role of inflammation triggers and cytokines, Front. Immunol. 9 (2018), https://doi.org/10.3389/fimmu.2018.00586.
[20] T. Tanaka, M. Narazaki, T. Kishimoto, Il-6 in inflammation, immunity, and disease, Cold Spring Harbor Perspect. Biol. 6 (2014), https://doi.org/10.1101/cshperspect.a016295.
[21] A.C. Lima, D. Amorim, I. Laranjeira, A. Almeida, R.L. Reis, H. Ferreira, F. Pinto-Ribeiro, N.M. Neves, Modulating inflammation through the neutralization of Interleukin-6 and tumor necrosis factor-α by biofunctionalized nanoparticles, J. Contr. Release 331 (2021), https://doi.org/10.1016/j.jconrel.2021.02.001.
[22] A.R. Guerreiro, I. Chianella, E. Piletska, M.J. Whitcombe, S.A. Piletsky, Selection of imprinted nanoparticles by affinity chromatography, Biosens. Bioelectron. 24 (2009), https://doi.org/10.1016/j.bios.2009.01.013.
[23] S. Ambrosini, S. Beyazit, K. Haupt, B. Tse Sum Bui, Solid-phase synthesis of molecularly imprinted nanoparticles for protein recognition, Chem. Commun. 49 (2013) 6746–6748, https://doi.org/10.1039/c3cc41701h.
[24] A. Poma, A. Guerreiro, M.J. Whitcombe, E.v. Piletska, A.P.F. Turner, S.A. Piletsky, Solid-phase synthesis of molecularly imprinted polymer nanoparticles with a reusable Template-"Plastic antibodies", Adv. Funct. Mater. 23 (2013) 2821–2827, https://doi.org/10.1002/adfm.201202397.
[25] P.X. Medina Rangel, S. Laclef, J. Xu, M. Panagiotopoulou, J. Kovensky, B. Tse Sum Bui, K. Haupt, Solid-phase synthesis of molecularly imprinted polymer nanolabels: affinity tools for cellular bioimaging of glycans, Sci. Rep. 9 (2019), https://doi.org/10.1038/s41598-019-40348-5.
[26] A. Cutivet, C. Schembri, J. Kovensky, K. Haupt, Molecularly imprinted microgels as enzyme inhibitors, J. Am. Chem. Soc. 131 (2009) 14699–14702, https://doi.org/10.1021/ja901600e.
[27] J. Xu, S. Ambrosini, E. Tamahkar, C. Rossi, K. Haupt, B. Tse Sum Bui, Toward a universal method for preparing molecularly imprinted polymer nanoparticles with antibody-like affinity for proteins, Biomacromolecules 17 (2016), https://doi.org/10.1021/acs.biomac.5b01454.
[28] P.J. Flory, Thermodynamics of high polymer solutions, J. Chem. Phys. 9 (1941), https://doi.org/10.1063/1.1750971.
[29] P.G. de Gennes, Scaling Concepts in Polymer Physics, Cornell university press, Ithaca N.Y., 1979.
[30] P.G. de Gennes, Dynamics of fluctuations and spinodal decomposition in polymer blends, J. Chem. Phys. 72 (1980), https://doi.org/10.1063/1.439809.
[31] J. Homola, S.S. Yee, G. Gauglitz, Surface plasmon resonance sensors: review, Sens. Actuators, B Chem. 54 (1999), https://doi.org/10.1016/S0925-4005(98)00321-9.
[32] N. Cennamo, D. Massarotti, L. Conte, L. Zeni, Low cost sensors based on SPR in a plastic optical fiber forbiosensor implementation, Sensors 11 (2011), https://doi.org/10.3390/s111211752.
[33] L. Pasquardini, N. Cennamo, G. Malleo, L. Vanzetti, L. Zeni, D. Bonamini, R. Salvia, C. Bassi, A.M. Bossi, A surface plasmon resonance plastic optical fiber biosensor for the detection of pancreatic amylase in surgically-placed drain effluent, Sensors 21 (2021), https://doi.org/10.3390/s21103443.

[34] D.v. Novikov, A.N. Krasovskii, Density-density correlations on a gelatin films surface, Phys. Solid State 54 (2012), https://doi.org/10.1134/S1063783412080239.
[35] M. Sun, X. Sun, Z. Wang, S. Guo, G. Yu, H. Yang, Synthesis and properties of gelatin methacryloyl (GelMA) hydrogels and their recent applications in load-bearing tissue, Polymers 10 (2018), https://doi.org/10.3390/POLYM10111290.
[36] B. Zhou, X. Jiang, X. Zhou, W. Tan, H. Luo, S. Lei, Y. Yang, GelMA-based bioactive hydrogel scaffolds with multiple bone defect repair functions: therapeutic strategies and recent advances, Biomater. Res. 27 (2023), https://doi.org/10.1186/s40824-023-00422-6.
[37] A.T. Young, O.C. White, M.A. Daniele, Rheological properties of coordinated physical gelation and chemical crosslinking in gelatin methacryloyl (GelMA) hydrogels, Macromol. Biosci. 20 (2020), https://doi.org/10.1002/mabi.202000183.
[38] F. Aliotta, V. Arcoleo, G. la Manna, V. Turco Liveri, Structural and dynamical investigation of gelatin containing water-in-oil microemulsions, Colloid Polym. Sci. 274 (1996), https://doi.org/10.1007/BF00656629.
[39] H. Hinterwirth, S. Kappel, T. Waitz, T. Prohaska, W. Lindner, M. Lämmerhofer, Quantifying thiol ligand density of self-assembled monolayers on gold nanoparticles by inductively coupled plasma-mass spectrometry, ACS Nano 7 (2013), https://doi.org/10.1021/nn306024a.
[40] C.E. Neri-Cruz, F.M.E. Teixeira, J.E. Gautrot, A guide to functionalisation and bioconjugation strategies to surface-initiated polymer brushes, Chem. Commun. 59 (2023), https://doi.org/10.1039/d3cc01082a.
[41] A.S. Holehouse, R.v. Pappu, Collapse transitions of proteins and the interplay among backbone, sidechain, and solvent interactions, Annu. Rev. Biophys. 47 (2018), https://doi.org/10.1146/annurev-biophys-070317-032838.
[42] R.v. Pappu, X. Wang, A. Vitalis, S.L. Crick, A polymer physics perspective on driving forces and mechanisms for protein aggregation, Arch. Biochem. Biophys. 469 (2008), https://doi.org/10.1016/j.abb.2007.08.033.
[43] D. Mukherji, C.M. Marques, K. Kremer, Polymer collapse in miscible good solvents is a generic phenomenon driven by preferential adsorption, Nat. Commun. 5 (2014), https://doi.org/10.1038/ncomms5882.
[44] T. Matsoukas, Statistical thermodynamics of irreversible aggregation: the sol-gel transition, Sci. Rep. 5 (2015), https://doi.org/10.1038/srep08855.
[45] P.X. Medina Rangel, A. Mier, E. Moroni, F. Merlier, L.A. Gheber, R. Vago, I. Maffucci, B. Tse Sum Bui, K. Haupt, Molecularly imprinted polymer nanogels targeting the HAV motif in cadherins inhibit cell-cell adhesion and migration, J. Mater. Chem. B 10 (2022), https://doi.org/10.1039/d2tb00680d.
[46] K. Sachin, V.H. Jadhav, E.M. Kim, H.L. Kim, S.B. Lee, H.J. Jeong, S.T. Lim, M. H. Sohn, D.W. Kim, F-18 labeling protocol of peptides based on chemically orthogonal strain-promoted cycloaddition under physiologically friendly reaction conditions, Bioconjug. Chem. 23 (2012), https://doi.org/10.1021/bc3002425.
[47] J. Chen, E.S. Garcia, S.C. Zimmerman, Intramolecularly cross-linked polymers: from structure to function with applications as artificial antibodies and artificial enzymes, Acc. Chem. Res. 53 (6) (2020) 1244–1256, https://doi.org/10.1021/acs.accounts.0c00178.
[48] S. di Masi, M. Costa, F. Canfarotta, A. Guerreiro, A. Hartley, S.A. Piletsky, C. Malitesta, An impedimetric sensor based on molecularly imprinted nanoparticles for the determination of trypsin in artificial matrices - towards point-of-care diagnostics, Anal. Methods 16 (2023), https://doi.org/10.1039/d3ay01762a.
[49] C. Herrera León, N.A. Kalacas, A. Mier, P. Sakhaii, F. Merlier, E. Prost, I. Maffucci, V. Montagna, H. Mora-Radó, P.K. Dhal, B. Tse Sum Bui, K. Haupt, Synthetic peptide antibodies as TNF-α inhibitors: molecularly imprinted polymer nanogels neutralize the inflammatory activity of TNF-α in THP-1 derived macrophages, Angew. Chem., Int. Ed. 62 (2023), https://doi.org/10.1002/anie.202306274.
[50] T. Zhang, M. Berghaus, Y. Li, Q. Song, M.M. Stollenwerk, J. Persson, K.J. Shea, B. Sellergren, Y. Lv, PSMA-targeting imprinted nanogels for prostate tumor localization and imaging, Adv. Healthcare Mater. 14 (2024), https://doi.org/10.1002/adhm.202401929.
[51] Y. Li, D. Yin, S.Y. Lee, Y. Lv, Engineered polymer nanoparticles as artificial chaperones facilitating the selective refolding of denatured enzymes, Proc. Natl. Acad. Sci. USA. 121 (2024), https://doi.org/10.1073/pnas.2403049121.
[52] L. Chen, X. Wang, W. Lu, X. Wua, J. Lia, Molecular imprinting: perspectives and applications, Chem. Soc. Rev. 45 (2016), https://doi.org/10.1039/C6CS00061D.
[53] T. Ren, B. Grosshäuser, K. Sridhar, T.J.F. Nieland, A. Tocchio, U. Schepers, U. Demirci, 3-D geometry and irregular connectivity dictate neuronal firing in frequency domain and synchronization, Biomaterials 197 (2019), https://doi.org/10.1016/j.biomaterials.2019.01.017.
[54] D. Nečas, P. Klapetek, Gwyddion: an open-source software for SPM data analysis, Cent. Eur. J. Phys. 10 (2012), https://doi.org/10.2478/s11534-011-0096-2.